UNIVERSITÀ DEGLI STUDI DI NAPOLI
FEDERICO II

Scuola Politecnica e
delle Scienze di Base

DI
C
Ma
PI
Dipartimento
di Ingegneria Chimica,
dei Materiali e della
Produzione Industriale
Università degli Studi
di Napoli Federico II

Università degli Studi di Napoli Federico II
Ph.D. Program in Industrial Products and Processes Engineering
XXXV Cycle

THESIS FOR THE DEGREE OF DOCTOR OF PHILOSOPHY

GIUSEPPE PORPORA

Experiments and Modelling of Solvent Sealing of Polymeric Films

SCUOLA POLITECNICA E DELLE SCIENZE DI BASE
DIPARTIMENTO DI INGEGNERIA CHIMICA, DEI MATERIALI E DELLA PRODUZIONE INDUSTRIALE

Experiments and Modelling of Solvent Sealing of Polymeric Films

Ph.D. Thesis presented
for the fulfillment of the Degree of Doctor of Philosophy
in Industrial Products and Processes Engineering
by

Giuseppe Porpora

December 2022

Approved as to style and content by

Advisors: Francesco Greco, Raffaele Pastore

Co-advisors: Andrea Gabriele

Università degli Studi di Napoli Federico II
Ph.D. Program in Industrial Products and Processes Engineering
XXXV cycle - Chairman: Prof. Andrea D'Anna

Candidate's declaration

I hereby declare that this thesis submitted to obtain the academic degree of Philosophiæ Doctor (Ph.D.) in Industrial Products and Processes Engineering is my own unaided work, that I have not used other than the sources indicated, and that all direct and indirect sources are acknowledged as references.
Parts of this dissertation have been published in international journals and/or conference articles (see list of the author's publications at the end of the thesis).

Napoli, March 10, 2023

Giuseppe Porpora

Abstract

Sealing of polymeric films is a widespread process, exploited in several industrial and technological applications, ranging from aeronautics to large consumer goods and bio-medical devices. Thus, the study of polymer/polymer interfaces and local polymer dynamics is currently raising a great deal of interest. Among several approaches, a modern way to promote the welding of two polymeric films is the absorption of a liquid solvent at the polymer surface: the so-called solvent-sealing technique. According to this method, a given amount of solvent is applied on a given polymeric film and, then, the wet film and the dry companion are put in contact, also applying pressure to promote the joint formation.

The objective of this Ph.D. project is to study the fundamentals of the solvent-sealing transformation, by investigating the nature of its two main steps: solvent diffusion and swelling of the film, and the adhesion process itself, laying the foundations for a predictive tool for the seal strength. The main target application is the sealing of Polyvinyl alcohol films for laundry detergent pods' production, where water is used as a solvent. The thesis combines experimental, theoretical and numerical tasks.

From an experimental perspective, solvent diffusion, film swelling and adhesion between polymer layers have been characterized for the system water-Polyvinyl alcohol by means of several techniques, including optical microscopy, optical coeherence tomography and peel tests.

From the theoretical and numerical side, a new model for solvent diffusion in a deforming polymer matrix has been developed and numerically solved. We demonstrate that the model provides fully satisfactory predictions by validating its outcomes both with our own experimental results and with literature data.

Keywords: anomalous diffusion, wet adhesion, solvent sealing

Contents

CHAPTER 1

Introduction

Sealing of polymeric materials is a widespread process, employed in several fields of industry, like recycling of thermosetting polymers [1], packaging and manufacturing of plastic pipes [2]. It is therefore clear why interest in studying polymer/polymer interfaces and the local polymer dynamics is rapidly growing. Sealing can be accomplished by different techniques, like through impact, heating or vibrations [3]. A modern way to improve the welding strength of two polymeric layers is through absorption of a solvent at the polymer surface: the so-called solvent-sealing technique [4, 5]. The solvent, indeed, can soften the adherend's surface, promoting the molecular mobility of polymer chains and the subsequent inter-diffusion across the interface.

Recently, a considerable interest has been growing specifically around the design of these adhesives in wet conditions, especially employing liquid solvents on the surfaces of polymer films. The field of applications ranges from aerospace industry to medical field, where the optimal biocompatibility of hydrated polymers and gels was exploited for wounds healing and tissues repair [6]. Moreover, it has been proved that, accurately tuning the solvent amount at the interface, a very strong joint can be obtained even if the contact of the two films lasts as short as 10 seconds

[7, 8]. This feature makes the process very appealing also for the field of large consumer goods, like Laundry Detergent Pods.

Laundry Detergent Pods are water-soluble pouches containing a predosed quantity of detergent. Their functioning is simple: the casing dissolves at contact with hot water in the washing machine, releasing the detergent and the perfumes. Pods production is, obviously, a continuous process. A film roll essentially made of Polyvinyl alcohol (PVA) is unwinded and the film is placed on a belt with cavities. Here, a vacuum machine deforms the polymeric material to make it adhere to the cavities' walls, obtaining the characteristic shape of the pod; this process is aided by a temperature increase of the system. Once the cavities are covered by the film, they can be filled with the detergent. At the same time, another film is wetted on one surface and, after just a couple of seconds (or so), the two companions are put one on the other, with a small pressure to promote intimate contact between the polymer chains. In this way, sealing will occur at cavities' edges, with the aim of avoiding detergent leaks from the pod. Finally, after only few seconds of contact, the pouches are cut and put into their package.

Obtaining a good seal quality (in such a small amount of time) is a key step in the process of pods' production, for several reasons, including:

- Legal Requirements: there is a legally required minimum strength to be reached. Such a limit has been set to avoid health risks for kids that could accidentally try to ingest the products;
- Consumer Experience: poor sealing can cause leaks, affecting not only the single faulty pod but the entire package. Detergent leaks constitute one of the biggest consumers' complaints;
- Unplanned Down Time: Leaks cause production stops due to the necessity to clean the plant, hence affecting the fabrication of new pods.

To examine the seal quality, a *rupture test* is used. Once a production batch is ready, the seal force of a statistically meaningful sample of pods is measured by squeezing them under a press, measuring the pressure at which the seal breaks. Such a test presents at least two disadvantages: it is indeed a destructive methodology that wastes a percentage of the final product, and it does not give insights on the causes of the possible bad sealing quality.

It would be thus useful to complement such a rupture test with a predictive tool for the sealing strength, based on the physical phenomena underlying the adhesion mechanism. The development of a predictive model has indeed several advantages.

First of all, such a model would take into account a given (ideally small) number of parameters and independent variables, identified as significant predictors of a high-quality sealing. These features could therefore be tested through controlled experiments on raw materials (e.g., the polymer film) *before* the actual pod is made, blocking upstream the production of faulty pouches. Moreover, if a variation on the process is proposed (e.g., to increase film solubility), the consequences on seal quality could be immediately evaluated. Finally, the design of new materials and the choice of the most effective operating conditions could be driven by the model, obtaining the best possible welding in a cost-efficient way.

In a bottom-up approach, the complete knowledge of wet adhesion mechanism relies on understanding and modelling: i) solvent diffusion in the polymer film, and ii) chains' motion across the interface, and, of course, the connections between those two processes.

Solvent absorption in polymer matrices is a complex issue that cannot be treated with the standard Diffusion Equation, due to the emergence of strong couplings between polymer and solvent. For instance, the polymer typically tends to increase its volume (swelling) to accommodate the penetrant molecules, and its deformation can, in turn, affect the diffusion. The interplay between these two phenomena gives rise to a wide range of peculiar effects: very often, for example, the solvent concentration profile shows sharp discontinuities. It is clear that such a property cannot be explained by classic Fick's equation, that predicts a smooth concentration profile; a different theory is thus needed. Up to date, however, no single model has been capable to enclose the variety of behaviours observed in these systems [9, 10] without employing a huge amount of parameters.

Regarding the adhesion itself, the main contribution to the joint formation is thought to be polymer entanglement, a largely studied phenomenon for which excellent theories are available [11]. However, the impact of the solvent presence can not be easily taken into account. Moreover, the largest part of the experiments to measure adhesion force relies on the breaking of the seal itself: this (stongly non-linear) approach leads to different force estimates depending on the adopted technique, especially for polymeric materials where viscoelastic phenomena play a huge role.

The aim of this work is to lay the foundations for understanding such an intricate problem in a PVA-water system of interest for pods' production. Our work mainly focuses on the first steps of the solvent assisted polymer sealing, namely diffusion and swelling. From an experimental perspective, this process has been characterized both optically (by means of Optical Microscopy and Optical Coherence Tomography) and gravimetrically, measuring the absorbed mass of solvent as a function of time. From a theoretical perspective, a new model has been developed that has been proven to be very versatile, correctly predicting diffusion and swelling behaviours not only in our system, but also in a range of different cases. It is emphasized that the model only requires a small set of measurable parameters. In addition, we have also investigated the second step of the process, namely the joint formation, by developing a protocol to perform reliable peel force measurements, under conditions strictly mimicking the real pods' production. Actual measurements to characterize the adhesion between the two polymer layers have been conducted, changing the operating conditions in a significant window.

The thesis is structured as follows.

Chapter 2 presents a literature review, mainly describing experimental features (and anomalies) of liquid solvent absorption in polymeric films. Some models, based on modifications of Fick's Second Law, are also presented, highlighting the different ways through which film deformation has been taken into account. The second section of this Chapter is devoted to the adhesion of two polymeric layers, and shows a simple prediction for seal force as a function of contact time of the two films in dry conditions.

Chapter 3 introduces the model we developed, and the way in which it has been conveniently solved. Excellent agreement between model outcomes and experimental data is shown, first for systems analyzed in previous works in the available literature [12, 8], and secondly, and more importantly, on the PVA-water systems of direct interest here.

In Chapter 4, materials and methods regarding the experimental part of the work have been widely discussed; results of these tests are reported in Chapter 5 and there compared with model predictions.

Finally, Chapter 6 summarizes the main achievements of this work and discusses the comparison among the model developed in Chapter 3 and some of the previous ones that were presented in Chapter 2.

CHAPTER 2

Background on Absorption/Swelling and Sealing

In this Chapter, a literature review describing the physical phenomena underlying the process of solvent sealing is presented.

Section 2.1 is dedicated to the transport of a low molecular weight solvent inside a polymer matrix: both the phenomenology and the available continuum mechanics models to describe the transport are presented.

The second section of this Chapter will provide instead a brief overview on the sealing process itself: a model is presented that tries to explain the mechanisms behind seal formation, and gives some predictions on the peel force dependence from control parameters.

2.1 Solvent Absorption in Polymer Films

The literature on solvent absorption in polymer films is quite vast since the technological and scientific interest about the subject started long time ago and never really switched off, due to both the huge importance of this process in industrial applications, and to the physical and mathematical challenges underlying the process itself. A comprehensive description of such vast amount of data and theories is far beyond the scope of this Chapter, that is instead to present the main experimental features occurring in this kind of systems, and of introducing and comparing the various modeling strands that gained the largest interest over the years, thus showing the connections among the ideas underlying these models. Extensive reviews can of course be found in literature [13, 14, 10, 15, 16, 17, 18, 19]; moreover, various research papers have wonderful introductory sections to describe both the key features of fluid sorption in polymers and the fundamental modeling approaches [20, 21]. Even if most of the described features are valid for both liquid and gas solvents, the main focus of this thesis is on liquid absorption.

2.1.1 Experimental Features

A wide range of experimental features in the absorption of low molecular weight solvents in polymer films has been observed, showing peculiarities and system-specific characteristics, both in the concentration profiles and in integral quantities like the absorbed mass.

One very often observed phenomenon is the emergence of two sharp advancing fronts in the mixture [22, 23, 24, 25]: the first one separates the solid part of the film from the hydrated area, and is usually termed *penetration* (or *hydration*) front, while the second is the interface between the swollen area itself and the solution, the so-called *swelling* front.

The position of these fronts as a function of time has been investigated, and two limiting cases were found: depending on several features of the polymer films, such as the glass transition temperature of the polymeric film, its thickness, and the orientation of polymer chains, the motion of these fronts is typically well-described by a square-root or a linear function of time. The position of these fronts, for example, has been found to increase as $t^{\frac{1}{2}}$ for unoriented [25, 26], thick [27] polymer films at a temperature above their glass transition [12]; on the other hand, a linear function of time has often been observed in films with a preferred chain direction [28], thin [27] and in a glassy state [12]. These must be merely interpreted as a rule of thumb, since exceptions are reported in literature to the above given cases [29].

Assuming a power-law for the position of these fronts as a function of time, the exponent of such power-law is the first element that has been used to create a classification of the types of solvent diffusion and swelling of the polymeric films. The categories that are still used today trace back to

Alfrey, Gurnee and Lloyd [30], who employed the term "Case I" diffusion to indicate a penetration front proportional to $t^{\frac{1}{2}}$ (which is a typical exponent observed in diffusion-driven processes), as opposed to "Case II" diffusion, characterized by a penetration front moving with a constant velocity (i.e. whose motion is linear with time). Moreover, other features have been recognized as being typical of "Case II" diffusion, namely:

- Negligible concentration gradient in the swollen area;
- Mass of absorbed solvent linear in time;
- Existence of a small "Fickian" precursor in the dry region;
- Existence of an induction time before the front motion starts.

While this distinction had been done considering the penetration front, it has later been shown that the swelling front shares the same time-dependence: $\propto t^{\frac{1}{2}}$ for Case I diffusion [8] and $\propto t$ for Case II diffusion [31].

Nowadays, the nomenclature employed in literature can be somehow confusing. The term "Fickian", for example, is sometimes used as a synonym for Case I diffusion; moreover the same word can also refer to Diffusion Equations with a diffusion coefficient depending on concentration. In this work, however, Case I diffusion is employed to designate a concentration profile containing discontinuities, while Fickian indicates a smooth concentration profile throughout the entire film, obtained solving Fick's second law (see subsection on Mathematical Modeling) with a *constant* diffusion coefficient. It is here noted, however, that, defining the front as the position at which concentration reaches a certain arbitrary threshold, the same power-law behaviour for Case I and Fickian diffusion is obtained for the hydration front. [32].

Case I and Case II diffusion are only limiting cases, and systems in which the position of penetration front is proportional to t^n with n being different from both 1 and 1/2 have been found [14] (Fig. 2.1): in this work this kind of diffusion is named *anomalous*.

The absorbed mass of solvent has also been analyzed as a function of time. While for Case I and Case II it shares the same power-law behaviour (with the same exponent) of the two fronts, a wide range of phenomena has

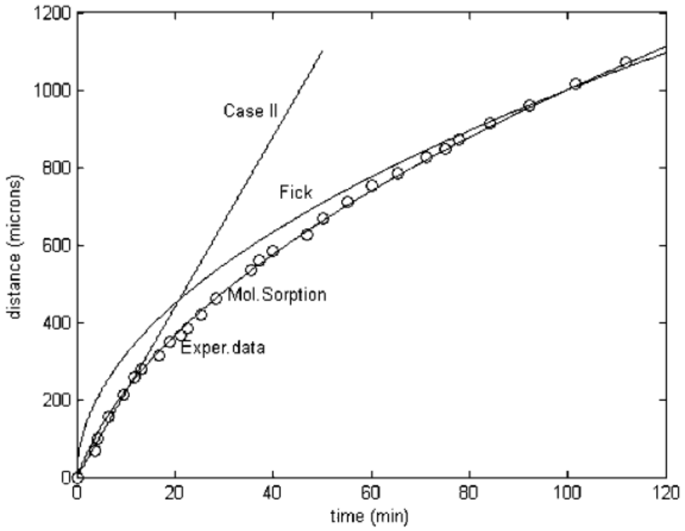

Figure 2.1. Measured position penetration front as a function of time for the system Polymethyl methacrylate-methanol. From [14]. The best power-law fit would lead to an exponent 0.64, thus showing anomalous diffusion.

been reported [15, 33, 34], with time-dependencies of the absorbed mass that are not necessarily coupled with the ones of the fronts:

- Case I: The mass absorbed by the film shows a square root function of time $M(t) \propto t^{\frac{1}{2}}$. Notice that this exponent for the mass is also characteristics of a standard Fickian Diffusion;
- Pseudo-Fickian: A Fickian behaviour is observed but only at short times; absorbed mass can thus be fitted by a power-law function with an exponent smaller than 0.5;
- Sigmoidal: Mass as a function of time is represented by a sigmoidal function;
- Two-stage: Sorption curves rapidly reach a quasi-equilibrium value, after which mass uptake increases towards true equilibrium;
- Case II: $M(t) \propto t$;

- Super Case II: Mass increases faster than linear have been observed (particularly in thin films);
- Overshoots: Overshoots above the equilibrium value are also observed.

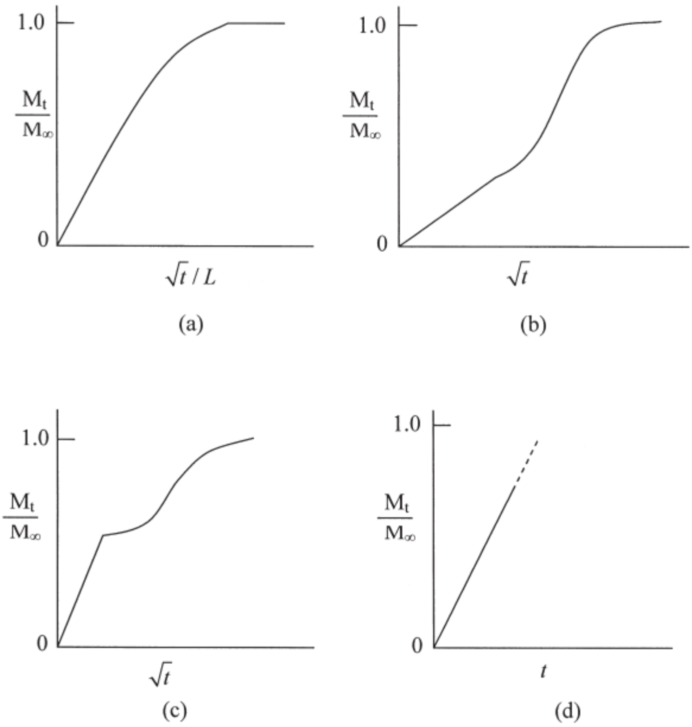

Figure 2.2. Some experimental behaviours observed in solvent uptake as a function of time, from [13]. (a) Case I; (b) sigmoidal; (c) two-stage; (d) Case II diffusion. Values of mass $M(t)$ are plotted divided by the equilibrium value M_∞.

To sum-up, as a parallel to the front position, solvent uptake has been modeled by a power-law function:

$$M(t) = At^B \tag{2.1}$$

when $B = 1$ the diffusion is termed Case II; when $B = \frac{1}{2}$ the diffusion is termed Case I; all other cases are called anomalous.

Investigating the causes of such a variety of behaviours, and understanding the key features at play in any of these presented cases, has been quite challenging and several authors proposed different mechanisms that could underlie these phenomena, as it is highlighted in Section 2.1.2. For many authors, the departure from classical Fickian diffusion could be ascribed to a non-negligible relaxation time of the polymer matrix. Vrentas and Duda [35, 36, 29] proposed in fact to define a *diffusion* Deborah number, defined as:

$$DEB = \frac{\lambda_m}{\tau_D} \tag{2.2}$$

Where λ_m is a polymer relaxation time and $\tau_D \propto \frac{H^2}{D}$ the diffusion time (with H the original film thickness, and D a diffusion coefficient). When $DEB << 1$, i.e., when the polymer relaxation time is negligibly small compared to the diffusion time, the transport could be considered as the one of a simple fluid in another one (and thus it can be modeled by classical fickian diffusion); when $DEB >> 1$ the penetrant molecule is essentially moving in an elastic or completely rigid solid, a situation that is also known for being adequately modeled by Fick's second law with a constant diffusion coefficient [35]; when the two times are of the same order of magnitude, $DEB \approx 1$ and the mixture shows non-fickian behaviour.

There are clear ambiguities in the definition given in eq. 2.2. Indeed, DEB is in general a function of penetrant concentration, since both the polymer relaxation time and the diffusion coefficient can change with solvent content. Vrentas et al. state that, ideally, the value of DEB should be checked both at beginning (essentially dry solid) and at the end (swollen polymer) of the diffusion process. When the value is consistently above or below unity, the standard diffusion equation can be used; changes in these values, instead, have been linked to non-Fickian diffusion.

To sum-up, the introduction of DEB is mainly a qualitative tool, but it correctly points out that, to describe the absorption process in polymers, coupling of mass transport and film deformation plays a key role. The next subsection aims at describing how different models tried to incorporate this concept in a mathematical framework.

2.1.2 Mathematical Models

As already mentioned, analyzing and comparing the plethora of existing models on the subject is far beyond the scope of this Chapter. To narrow the field, models consisting in hyperbolic equations ([37, 38]) are not considered here, and only modifications of the standard parabolic diffusion equation are presented. Moreover, since in our process the time span going from water application to the contact of the two films is very short, film dissolution is not taken into account (for this subject, see for example [39, 40, 41] and references therein). Models are here described as they were first introduced: for this reason most of them will be presented in a one-dimensional form.

The mathematical foundation to describe mass transport in a continuum-mechanic approach is the diffusion equation:

$$\frac{\partial c}{\partial t} = D\nabla^2 c \tag{2.3}$$

with c being the concentration of one species, t the time, ∇^2 the Laplacian operator and D the *constant* diffusion coefficient. Equation 2.3 is also known as Second Fick's Law since it was firstly introduced by Adolf Fick [42] as an heuristic analogy between heat conduction and mass transport.

To obtain Eq. 2.3, the starting point is of course the mass balance:

$$\frac{\partial c}{\partial t} = -\nabla \cdot \mathbf{j} \tag{2.4}$$

with $\mathbf{j}$ being the flux per unit time and area, and $\nabla\cdot$ the divergence operator. Fick assigned the following constitutive equation for the flux, usually called Fick's First Law:

$$\mathbf{j} = -D\nabla c \tag{2.5}$$

(D is here a given constant). It is thus assumed that the driving force for diffusion is the concentration gradient ∇c. Diffusion equation 2.3 is a very powerful tool and has been proved to correctly predict the concentration profile in various systems; moreover, analytical solutions are available in various geometries [9].

Several attempts have been made to modify such equation in order to account for non-fickian features. Earliest attempts were introduced by

Crank. He, for example, proposed to consider a history-dependent diffusion coefficient $D = D(c,t)$ in eqq. 2.4-2.5, obtained through the additional equation [43]:

$$\frac{\partial D}{\partial t} = \left(\frac{dD_i(c)}{dc}\right)\left(\frac{\partial c}{\partial t}\right) + \alpha(c)(D_e(c) - D) \tag{2.6}$$

where D_i is the part of D that should reflect an instantaneous change in polymer conformation when the contact with solvent occurs, D_e is a local (putative) equilibrium value of the diffusion coefficient, and α is a parameter that controls the approach rate to the equilibrium. This model was used to describe curves of solvent uptake in the system methylene chloride-polystyrene at room temperature, but does not present sharp discontinuities in the concentration profile. The easiest way to obtain such a discontinuity was again indicated by Crank, with a simple modification of equation 2.3. Notably, he introduced a discontinuity in the diffusion coefficient [9]:

$$\begin{cases} D = D_{02} & 0 \leq c \leq c_h \\ D = D_{01} & c_h \leq c \leq c_\infty \end{cases} \tag{2.7}$$

where c_h is the concentration at the discontinuity, and c_∞ is the concentration at the solvent-polymer interface. Results of this approach are illustratively shown in Fig. 2.3.

In a way or another, the simple concepts introduced by Crank are found in the majority of later works.

Weakly coupled models

The first models here presented are labelled, following Ref. [10], as weakly coupled models, since film deformation is not directly taken into account as an independent variable, but there is an effect of the stretching on solvent diffusion. Three different models are here presented: the model by Petropoulos et al., the model by Thomas and Windle, and the one by Astarita and Sarti.

Petropoulos et al. The model by Petropoulos et al. [44, 45] still relies on mass balance 2.4 (in its 1D version) but the chemical potential gradient

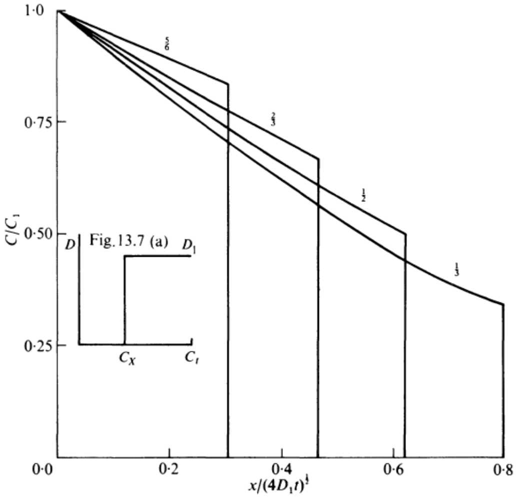

Figure 2.3. Concentration profile as a function of dimensionless distance, obtained via Standard Diffusion Equation and a discontinuous diffusion coefficient. Curves are self-similar in time and parametric in c_h/c_∞. The case here represented is the one with $D_{02} = 0$, see inset.

$\frac{\partial \mu}{\partial x}$ (instead of the concentration gradient) is assumed as the driving force for sorption:

$$\frac{\partial C}{\partial t} = \frac{\partial}{\partial x}\left(\frac{D_T}{RT} C \frac{\partial \mu}{\partial x}\right) \tag{2.8}$$

Here, D_T is the thermodynamic diffusion coefficient, related to the the binary diffusion coefficient D by $D = D_T \frac{\partial lna}{\partial lnC}$ [16], C is the molar solvent concentration per unit volume of dry polymer, R the universal gas constant, T the temperature, and x is the spatial position along the slab, defined in a polymer-fixed frame of reference, with $x = 0$ indicating the interface between pure solvent and hydrated film at any time. Such equation has been recognized as a valid extension of Fick's Second Law, and it constitutes the basis of several models for sorption in polymer films.

Using $\mu = \mu_0 + RTln(a)$, with a being the solvent activity, and μ_0 a reference chemical potential, Eq. 2.8 becomes:

$$\frac{\partial C}{\partial t} = \frac{\partial}{\partial x}\left(D_T \frac{C}{a}\frac{\partial a}{\partial x}\right) \tag{2.9}$$

In this model $D_T = D_T(C)$ is some function of the concentration (polynomial or exponential, tipically). In a somehow analogous way as far as the "history dependence" introduced by Crank through Eq. 2.6, the model by Petropoulos et al. considered the following "constitutive equation":

$$\frac{\partial C}{\partial t} = \left(\frac{dC_0}{da}\right)\left(\frac{\partial a}{\partial t}\right) + \beta(C)(C_\infty - C) \tag{2.10}$$

with C_0 and C_∞ being the sorption isotherms for the unrelaxed and fully relaxed polymer, respectively, and $\beta(C)$ is usually assumed to increase exponentially with concentration. This model is capable to predict several non-Fickian features, including the presence of sharp fronts and Case II diffusion behaviour [45].

Concerning Petropoulos model and, to be precise, also Crank history-dependent model, it should be clearly evidentiated how both approaches contain a differential equation in time for an additional field (a and D, respectively), the physical origin of which is however obscure. Moreover, both models require three additional functions (D_i, D_e, α for Crank and C_0, C_∞, β for Petropoulos) that are given ad-hoc to attain the desired features of the solution.

Thomas and Windle Thomas and Windle theory [12, 46] is probably the most famous for solvent absorption and swelling in polymer films. The main equation is the same as for the model by Petropoulos et al., i.e., eq. 2.9, but they use a different "constitutive equation". Thomas and Windle, indeed, consider the solvent activity a as a function of solvent concentration *and*, in addition, of a solvent-induced "non-equilibrium osmotic pressure" Π, for which a formal constitutive equation called "Newton's law" was assumed:

$$\Pi = \eta \frac{\partial \epsilon}{\partial t} \tag{2.11}$$

where ϵ is the film stretching and $\eta = \eta_0 e^{KC}$ is the film viscosity, assumed to be an exponential function of the concentration (η_0 and K are constant).

This model is important because it explicitly recognizes the central role of film deformation in the absorption process. It is, however, still classified as a weakly coupled model, because, in the ensuing formulation of the model, deformation is assumed to be linked to concentration through an unknown constant (hence, an additional parameter) s:

$$\epsilon = sC \tag{2.12}$$

Thus, the equation coupled to eq. 2.9 in Thomas and Windle model is:

$$\frac{\partial C}{\partial t} = \frac{\Pi}{\eta s} \tag{2.13}$$

where, however, Π is still an unknown constitutive function, to be assigned. By a convenient (but arbitrary) choice for Π, an equivalent of eq. 2.10 is obtained:

$$\frac{\partial C}{\partial t} = \frac{-RT}{\nu N_A s \eta_0} ln \left(\frac{C}{a} \right) \exp\left(-KC\right) \tag{2.14}$$

where ν is the volume of a solvent molecule and N_A is the Avogadro constant. Thomas and Windle model can predict a wide range of phenomena, going from Case I to Case II diffusion, especially if the diffusion coefficient D_T is assumed to exponentially increase with concentration; however even if it is taken as a constant, sharp fronts still appear [12].

Due to such versatility with a relatively small amount of adjustable parameters, Thomas and Windle model has been variously re-interpreted and modified [47, 48, 49, 50, 51]. In particular, Durning et al. [47, 48] assumed a viscoelastic relaxation through a Maxwell equation in place of equation 2.11:

$$\Pi + \tau \left(\frac{\partial \Pi}{\partial t} \right) = \eta \frac{\partial \epsilon}{\partial t} \tag{2.15}$$

where τ represents a polymer relaxation time. Notwithstanding the introduction of a novel parameter, namely the relaxation time in the "constitutive equation" for the osmotic pressure, however, the description by Durning et al. remains simpler than the one by Petropoulos (see the discussion in [45]).

It is worth noting that, for all the weakly coupled models discussed so far, the (hidden) assumption is made that the local free energy of the system is a function of the time derivative of the concentration.

Astarita and Sarti Astarita and Sarti [52] proposed a different approach to the problem: the existence of a sharp front moving inside the polymer film is assumed a priori, and the front motion is given by an equation resembling chemical reactions:

$$\frac{d\Lambda}{dt} = K(c - c^*)^n \tag{2.16}$$

with Λ being the position of the discontinuity, c^* a "critical" concentration and n the order of the "chemical reaction". This equation must be coupled with the classical diffusion equation (Eq. 2.3 in its 1D formulation) and with the boundary conditions:

$$x = 0, \quad \forall t, \quad c = c_0 \tag{2.17}$$

$$x = \Lambda(t), \quad -D\frac{\partial c}{\partial x} = c\frac{d\Lambda}{dt} \tag{2.18}$$

leading to a moving boundary problem, since the position of the front has to be determined together with the concentration.

This hyper-stylized model is, as a matter of fact, based on an underived equation for the front motion, containing c^* as an unknown parameter. The model, however, has the merit of including a minimum number of parameters. Furthermore, although polymer deformation is in fact not explicitly considered, the model picks up as a fundamental quantity the hydration front motion; this will be a main point in the more complete strongly-coupled models.

Strongly coupled

Quite recently, a considerable interest has been growing around the explicit coupling of diffusion and deformation, particularly for the case of the gels [53, 54, 55, 56, 57, 58], with the deformation of the film considered to be an independent variable. These theories, termed strongly coupled [10], share several features: here only the model by Hong et al. [56] is described. Equations are written in non-Eulerian coordinates, where the following mass balance holds:

$$\frac{\partial C}{\partial t} = -\nabla_R \cdot \mathbf{J} \tag{2.19}$$

C is the solvent number concentration per unit volume of dry polymer, $\nabla_R \cdot = \frac{\partial}{\partial \mathbf{X}} \cdot$ is the divergence operator, and $\mathbf{J}$ is the number flux of molecules of solvent per unit time and area, for which the constitutive equation:

$$\mathbf{J} = -\mathbf{M} \cdot \nabla_R \mu \tag{2.20}$$

is used. Thus, also in this case, the driving force is the chemical potential gradient but, differently from the weakly coupled models, the mobility tensor $\mathbf{M}$ is, in general, a function of both the concentration C and the deformation gradient tensor $\mathbf{F}$ (see below, in Chapter 3): $\mathbf{M} = \mathbf{M}(C, \mathbf{F})$. The constitutive equation chosen for the chemical potential by Hong et al. is the Flory-Rehner [59] equation that, implying additivity of the volumes of the two species, creates a direct link between deformation and solvent concentration:

$$1 + \nu C = det(\mathbf{F}) \tag{2.21}$$

Notice that assuming volume additivity is not strictly necessary: Govindjee and Simo [60], for example, allowed for the volume of mixture to be smaller than the sum of the volumes of its pure components.[1]

While Govindjee and Simo explicitly showed the presence of sharp fronts in the concentration obtained with the theory they developed [61] (that is also capable to reproduce Case II behaviour), this is not the case for Hong et al., especially because they focused on gel applications, more than hydration of an initially dry polymer, where fronts are more likely to occur. However, very recently, this model was extended by Mao et al. [8]. In their work, like in the one of Astarita and Sarti, the presence of a sharp front was assumed a priori, dividing an hydrated region of the film from another considered essentially dry. The position of this front was assumed to move as a square root function of time (i.e., this is a model for Case I diffusion only), and the model by Hong et al. was assumed to hold in both

---

[1] An interesting discussion among the authors of these two models can be found at: http://imechanica.org/node/2487

regions, hydrated and dry, with the magnitude of the mobility tensor in the dry part being much smaller than the one in the hydrated side. The theory by Mao et al. is quite effective in predicting swelling behaviour of polymer films, in spite of using a limited set of parameters. For this reason, we took inspiration right from the Mao model in developing a new model that is able to capture also anomalous and Case II diffusion, while further reducing the number of needed parameters at the same time.

2.2 Adhesion of Polymer Surfaces

Adhesion of Polymer Surfaces is a quite challenging problem, since it involves several phenomena occurring on different length and time-scales. Several reviews [62, 63, 64, 65] highlighted the underlying mechanisms that promote adhesion. It is usually recognized that molecule bonding via chemical, physical and topological bonds is the principal contribution to the adhesion force: particularly, the entanglements formed between chains originally belonging to the two different films strongly impact the final joint strength.

Measurements of the adhesion force can be performed through several tests [65] and different experimental setups lead to discrepancies in the measured force, since viscoelastic phenomena play a key role [62].

Among the various possible experimental procedures, lap shear and peel tests have widely been used [66] to characterize adhesion between polymer layers. In both these tests, after bonding has occurred, the two films are pulled apart, measuring the force needed for the separation. The difference between lap shear experiments and peel tests stays in the direction in which the displacement of the two films occurs: in the former approach, the films are pulled away from each other following a direction parallel to the plane containing the two films, whereas in the latter, the separation direction is perpendicular to the aforementioned plane (see Fig. 2.4).

These standard tests, however, are not appropriate to measure the strength in our case, since they require that the sample is fully prepared before the actual measurement; in other words, this kind of measurements are made directly on the finite product. In solvent-sealing, however, as it was discussed above, both the time span going from water application

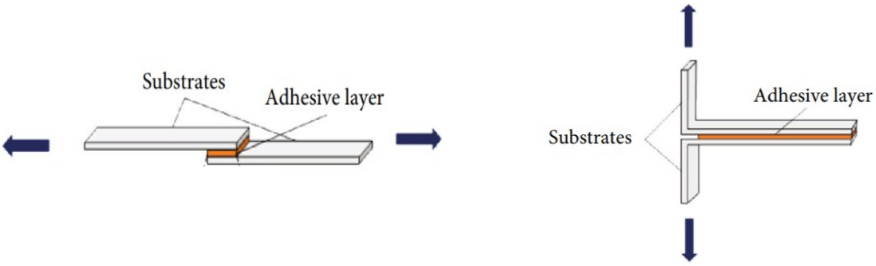

Figure 2.4. Lap shear (left) and peel (right) tests to measure adhesion strength in polymer films. Adapted from [67].

to films' combining (open time) and the time of contact of the two films (curing time) play a huge role in contributing to the seal strength, and we want to obtain the measure of such a strength "on-the-fly". For this reason, sample "preparation" and measurements should be performed one right after the other, and open and curing time should be, ideally, adjustable parameters.

A novel experimental protocol, closely resembling the solvent-sealing process occurring in the industrial production of laundry detergent pods, has thus been developed (see Chapter 4). As a consequence of the necessity of creating a protocol for this kind of measurements, the set of experiments presented in this thesis is limited and has to be considered as a preliminary study; in the operating window identified in our protocol, only two values of curing time have been investigated, which however are within the curing time window of the actual process (between 1 and 2 seconds).

This stated, this section is closed by presenting a prediction for the peel force as a function of the curing time, i.e. the time of contact of the two films prior to peeling.

The prediction for peel force is described using the chain pull-out model by Wool [3, 68], due to its simplicity. As a first step, a mechanism for joint formation is presented. Reptation model [11] is employed to describe the disentanglement of a single chain from the others in the film. Once a tail of the chain, called *minor chain* in [3], escapes from its initial tube, it is assumed to diffuse in a Fickian manner, and thus its length l increases as a square-root function of time:

$$l(t) \propto t^{\frac{1}{2}} \tag{2.22}$$

The minor chain can diffuse along the interface between the two films and create new entanglements with the chains of the other film, forming the joint. Its length is, thus, a fundamental parameter to predict the seal force as a function of curing time.

The seal breaking is then modelled in an ideal scheme, where the two films are pulled apart by applying a stress σ (supposedly uniaxial), and the only possible way to disjoint the films is assumed to be by pull-out of the chain from the tube create by entanglements: if U_c , the strain energy density per unit segment, is greater than U_p, i.e. the energy density to pull-out a chain from its tube, the seal is broken. Since it can be shown that $U_c \propto \sigma^2 l$ and $U_p \propto l$, the critical fracture stress (and thus the peel force P_f) at which $U_c = U_p$ is given by:

$$\sigma_c(t) \propto P_f(t) \propto \sqrt{l(t)} \propto t^{1/4} \tag{2.23}$$

where t is the curing time. Despite the simplicity in its derivation, 2.23 shows a good agreement with experimental data [3, 69]; nevertheless the eventual presence of a solvent and its role is not taken into account: in Chapter 5 results of "on-the-fly" T-peel tests are compared with this prediction, showing that such a monotone dependency is not sufficient to describe peel force in wet adhesion mechanism.

CHAPTER 3

Model Development and Applications

This Chapter is divided into two sections. Section 3.1 introduces a new model that has been developed to describe liquid solvent absorption (and consequent swelling) in polymeric matrices, and shows how such model is conveniently solved in an appropriate frame of reference. Section 3.2 shows the successful application of this model to predict diffusion and swelling behaviour in three different scenarios, i.e., Case I, Case II (drawing on literature data), and anomalous diffusion (for a PVA-water system analyzed in Chapter 4).

3.1 Model Development

The premises of the model that will be developed in this section closely follow references [56, 8], introduced in the previous Chapter. As we already discussed, solvent diffusion in polymer matrices very often occurs with the appearance of two sharp fronts: the hydration front that separates the hydrated area from the dry one, and the swelling front, in between the hydrated region and the pure solvent. In the model developed in this chapter, the position of the hydration front is assumed to be known at any time, and there is no limitation at all on the evolution in time of such a position; hence, it might also not be a power-law function.

The equations are introduced in Eulerian coordinates and then transformed in a novel, peculiar description, which proves more convenient from the mathematical point of view. In a lab-fixed frame of reference, indeed, the domain will change with time on both sides, i.e., penetration and swelling, in ways to be determined. The choice of the novel set of coordinates, instead, allows one to deal with a single unknown function describing the overall hydrated part of the film, thus much simplifying the involved math.

3.1.1 Eulerian Description

In a binary, isothermal, non-reacting mixture, the mass balance on a single species reads [70]:

$$\frac{\partial c_1}{\partial t} = -\nabla \cdot (c_1 \mathbf{v}_1) \tag{3.1}$$

where c_1 is the number concentration of molecules of species 1, $\mathbf{v}_1$ is its velocity and $\nabla \cdot = \frac{\partial}{\partial \mathbf{x}} \cdot = (\frac{\partial}{\partial x}, \frac{\partial}{\partial y}, \frac{\partial}{\partial z}) \cdot$ is the divergence operator in Eulerian coordinates. In the following, subscript 1 indicates molecules of solvent. Defining the number flux of solvent molecules per unit time and area as $\mathbf{j}_1 = c_1(\mathbf{v}_1 - \mathbf{v})$, with $\mathbf{v}$ being the average velocity of the mixture [71], Eq. 3.1 can be rewritten as:

$$\frac{\partial c_1}{\partial t} = -\nabla \cdot \mathbf{j}_1 + \nabla \cdot (c_1 \mathbf{v}) \tag{3.2}$$

Following [72], we shall consider here only the case where "there is no macroscopic motion in the fluid except that which may be caused by [...] concentration gradients. The velocity of this motion is proportional to the gradients, and terms [...] which involve the velocity are therefore quantities of the second order, and may be neglected". Thus we have:

$$\frac{\partial c_1}{\partial t} = -\nabla \cdot \mathbf{j}_1 \tag{3.3}$$

To close the problem, a constitutive equation is now needed, to link the flux to the unknown concentration field: $\mathbf{j}_1 = \mathbf{j}_1(c_1)$. Expressing $\mathbf{j}_1$ in terms of $\mathbf{v}$ is indeed purely formal, since of course $\mathbf{v}$ is unknown. In the framework of linear irreversible thermodynamics, a linear relationship between the flux and the thermodynamic force, i.e. the chemical potential gradient [56], holds:

$$\mathbf{j}_1 = -\frac{D(c_1)}{k_B T} c_1 \nabla \mu_1 \tag{3.4}$$

where k_B is the Boltzmann constant, T is the temperature and the chemical potential has been defined as the derivative of the Helmholtz free energy per unit volume, w, with respect to the number concentration of solvent molecules:

$$\mu_1 \equiv \frac{\partial w}{\partial c_1} \tag{3.5}$$

Thus, to close the problem, a relationship must be given between the chemical potential and the concentration field $\mu_1 = \mu_1(c_1)$, to finally find c_1 as a function of time and space. In the following section, such a relationship will be directly expressed in a novel, more convenient, set of coordinates, as anticipated.

3.1.2 Non-Eulerian Description

The new coordinates will be indicated by upper case letters $\mathbf{X}$. In this description, $\mathbf{X}$ and t are regarded as the independent variables, rather than $\mathbf{x}$ and t. The transformation $\mathbf{x} = \mathbf{f}(\mathbf{X}, t)$ gives the link between the two sets of coordinates [73]. Its gradient, a deformation gradient tensor, is defined as:

$$\mathbf{F}(\mathbf{X}, t) \equiv \nabla_R \mathbf{f}(\mathbf{X}, t) = \frac{d\mathbf{x}}{d\mathbf{X}} = \left(\frac{\partial x_i}{\partial X_j} \right) \tag{3.6}$$

In such a description, the mass balance reads as:

$$\frac{\partial C_1}{\partial t} = -\nabla_R \cdot \mathbf{J}_1 \tag{3.7}$$

Here, $C_1 = c_1/det(\mathbf{F})$ is the "new" number concentration of solvent, hence $C_1 = C_1(\mathbf{X}, t)$; $\nabla_R \cdot = \frac{\partial}{\partial \mathbf{X}} \cdot = (\frac{\partial}{\partial X}, \frac{\partial}{\partial Y}, \frac{\partial}{\partial Z}) \cdot$ is the divergence operator; $\mathbf{J}_1$ is the number flux of solvent molecules, per unit time and area. The definition of $\mathbf{J}_1$ is given through Nanson's formula [74]:

$$\mathbf{j}_1 \cdot d\mathbf{a} = \mathbf{j}_1 \cdot (det(\mathbf{F}))\mathbf{F}^{-T} \cdot d\mathbf{A} \equiv \mathbf{J}_1 \cdot d\mathbf{A} \tag{3.8}$$

with $d\mathbf{a}$ and $d\mathbf{A}$ the eulerian and non-eulerian elementary areas, respectively. The eulerian flux is thus related to the non-eulerian one via:

$$\mathbf{j}_1 = \frac{\mathbf{F} \cdot \mathbf{J}_1}{det(\mathbf{F})} \tag{3.9}$$

Constitutive equation 3.4 reads as:

$$\mathbf{J}_1 = -\frac{D(C_1)}{k_B T} C_1 \mathbf{F}^{-1} \cdot \mathbf{F}^{-T} \cdot \nabla_R \mu_1 \tag{3.10}$$

To express the chemical potential as a function of concentration, the classical Flory-Rehner theory is here exploited. The Helmholtz free energy is thus considered to be a sum of two contributions: one due to mixing of the two components, w_m, and the other one due to network stretching, w_s [75, 76]. The mixing term is described by the classical Flory-Huggins theory for polymer solutions, in the limit of an infinite polymerization degree [77]:

$$w_m = \frac{k_B T}{\nu(1-\phi_1)}(\phi_1 ln\phi_1 + \chi\phi_1(1-\phi_1)) \tag{3.11}$$

where χ is the polymer-solvent interaction parameter and ϕ_1 is the solvent volume fraction, that can be written in terms of C_1 and of the volume of a solvent molecule ν as [53]:

$$\phi_1 = \frac{\nu C_1}{1 + \nu C_1} \tag{3.12}$$

The stretching contribution is expressed as:

$$w_s = \frac{1}{2} N k_B T \left[\lambda_x^2 + \lambda_y^2 + \lambda_z^2 - 2ln(\lambda_x \lambda_y \lambda_z) - 3 \right] \tag{3.13}$$

with N being the number of polymer sub-chains per unit volume. Indeed, eq. 3.13 is written by thinking to a polymeric network, with sub-chains between chemical/physical crosslinks. λ_i are the stretches along i-th axis:

$$\lambda_i = F_{ii} = \frac{\partial x_i}{\partial X_i} \tag{3.14}$$

(no sum over repeated indices is assumed). Notice that, in eqq. 3.11 - 3.14, variables ϕ_1 and λ_i are not constant values at equilibrium: they are, in fact, fields $\phi_1 = \phi_1(\mathbf{X}, t)$, $\lambda_i = \lambda_i(\mathbf{X}, t)$. Flory-Rehner theory is however assumed to stay valid, as long as these variables are defined on a local, *elementary* volume: on a lattice, for example, this volume could be thought of as made up of a small number of cells.

Notice further that the assumption of Flory-Rehner lattice theory implies that there is no free volume inside the mixture, with any of the cells being occupied by either a network monomer or a water molecule. Thus, the total volume of the mixture is given, at any time, as the sum of the volume of the dry polymer matrix and the absorbed solvent volume. All of this is translated in the so-called incompressibility condition:

$$1 + \nu C_1 = det(\mathbf{F}) \tag{3.15}$$

Relation 3.15 is very handy, since it creates a link between the film deformation and the solvent concentration. Such a connection is fundamental, but the problem is still not mathematically closed. Eq. 3.13, indeed, introduces three new unknown variables (λ_x, λ_y, λ_z), and the incompressibility condition does not create a one-to-one relation between them and the concentration, at least not in the general case.

In the general case, in fact, further assumption on the kind of deformation occurring for the sample must be introduced. In the next subsections, model equations here presented will be specified for our target application, where the dimensionality can be reduced to 1, and the problem will be fully determined.

3.1.3 One dimensional case

Starting from this subsection on out, the subscript 1 is dropped for the quantities associated to solvent species. Assuming a one-dimensional transient swelling, $\lambda_y = \lambda_z = 1$ and the incompressibility condition becomes:

$$\lambda \equiv \lambda(X, t) = 1 + \nu C \tag{3.16}$$

Mass balance and constitutive equation for the flux are rewritten as:

$$\frac{\partial C}{\partial t} = -\frac{\partial J}{\partial X} \tag{3.17}$$

$$J = -\frac{D(C)}{\nu k_B T}\frac{\nu C}{(1+\nu C)^2}\frac{d\mu}{dX} \tag{3.18}$$

while the Flory-Rehner constitutive equation becomes:

$$\begin{aligned} w = w_m + w_s = \\ = \frac{k_B T}{\nu(1-\phi_1)}(\phi ln\phi + \chi\phi(1-\phi)) + \frac{1}{2}Nk_B T(\lambda^2 - 1 - 2ln\lambda) \end{aligned} \tag{3.19}$$

In 1D, the problem is thus closed, since, using 3.16 and definition 3.12, the Helmholtz free energy per unit volume can be written as a function of C only:

$$\begin{aligned} w = k_B T C\left(ln\frac{\nu C}{1+\nu C} + \frac{\chi\nu C}{1+\nu C}\right) + \\ +\frac{1}{2}Nk_B T((1+\nu C)^2 - 1 - 2ln(1+\nu C)) \end{aligned} \tag{3.20}$$

Using the definition $\mu = \frac{\partial w}{\partial C}$, the expression for the chemical potential as a function of concentration is finally found:

$$\begin{aligned} \mu = k_B T\left[ln\left(\frac{\nu C}{1+\nu C}\right) + \frac{1}{1+\nu C} + \frac{\chi}{(1+\nu C)^2}\right] + \\ +Nk_B T\nu\left(1+\nu C - \frac{1}{1+\nu C}\right) \end{aligned} \tag{3.21}$$

The problem is now closed, since equations 3.18 and 3.21 express the flux as a function of the solvent concentration C only. Once the function $D = D(C)$ is given, the mass balance 3.17 can be solved for given initial and boundary conditions.

3.1.4 Hydration of an initially dry polymer network

The model just presented describes liquid solvent diffusion in a mixture in which the other component is a polymer network, for example a gel. Now the equations will be specified for the case in which an essentially dry polymer film enters in contact with a liquid. As already mentioned, the hydration causes the emergence of a sharp front beyond which the solvent quantity is nearly zero. The total time span considered in our target application will be short enough to avoid the complete hydration of the slab, that can thus be considered a semi-infinite medium. The position of the hydration front is denoted by x_h in Eulerian coordinates and by X_h in non-Eulerian ones (Fig. 3.1). The Eulerian position of the penetration front, which is (in principle) directly measurable in the lab-fixed frame of reference, will be the only input needed to the model (see below, the subsection "ODE Formulation").

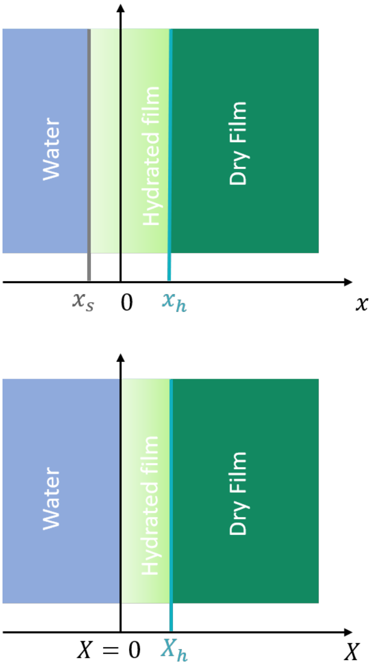

Figure 3.1. Representation of film hydration in Eulerian and non-Eulerian coordinates.

Regarding the other front, i.e., the swelling front, its position is denoted by x_s in Eulerian coordinates, while it will be in the origin of non-Eulerian coordinates, $X = 0$, for any time. Thus, the only unknown function describing the volume of the hydrated film is now $X_h(t)$. Once the problem will be solved in non-Eulerian coordinates, however, the distance $|x_s|$ will be given by equation 3.22:

$$|x_s(t)| = \int_0^{X_h(t)} (1 + \nu C(X,t))dX - x_h(t) \tag{3.22}$$

in this way, even if the problem is solved in a non-Eulerian description, the Eulerian swelling will of course always be available.

At the swelling front, i.e., $X = 0$, the hydrated film will be always in contact with pure water. Assuming thermodynamic equilibrium across the interface, and conventionally setting the chemical potential of pure water to zero, the following equation is obtained:

$$\frac{ln(\nu C_\infty)}{1+\nu C_\infty} + \frac{1}{1+\nu C_\infty} + \frac{\chi}{(1+\nu C_\infty)^2} + N\nu(1+\nu C_\infty - \frac{1}{1+\nu C_\infty}) = 0 \tag{3.23}$$

Solving Eq. 3.23, the concentration at equilibrium C_∞, i.e., the concentration at the water-polymer interface, can be calculated.

To mathematically describe the sharp hydration front, the diffusion coefficient is assumed to be discontinuous: it decreases exponentially in the hydrated region from a value $D_{01} = D_1(C_\infty)$, whereas it goes to a constant value $D_{02} << D_{01}$ in the dry side (Fig. 3.2):

$$\begin{cases} D = D_{02} & 0 \leq C \leq C_h \\ D \equiv D_1 = D_{01} e^{M\nu(C - C_\infty)} & C_h \leq C \leq C_\infty \end{cases} \tag{3.24}$$

with M being a positive dimensionless constant value.

The introduction of this discontinuity allows us to uncouple the equations, solving independently for the dry and the hydrated sides of the film.

In the hydrated side, the mass balance will be, substituting eq. 3.21 in eq. 3.18, and then this expression for the flux in eq. 3.7:

$$\frac{\partial C}{\partial t} = D_{01} \frac{\partial}{\partial X} \left[\xi(C) \frac{\partial C}{\partial X} \right] \tag{3.25}$$

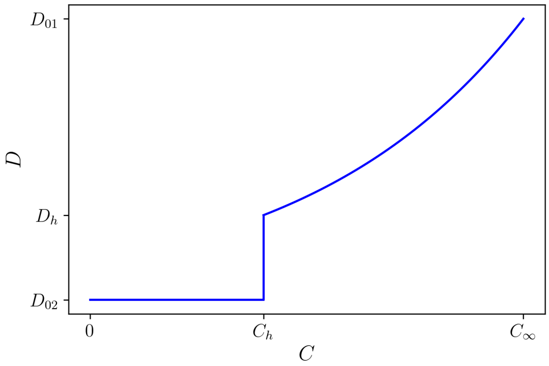

Figure 3.2. Diffusivity as a function of water concentration C.

where

$$\xi(C) = e^{M\nu(C-C_\infty)} \cdot \left(\frac{1}{(1+\nu C)^4} - \frac{2\chi\nu C}{(1+\nu C)^5} + N\nu \frac{\nu C((1+\nu C)^2+1)}{(1+\nu C)^4} \right) \tag{3.26}$$

In the dry side, where the matrix is essentially a solid and water diffusion has a very limited rate, Flory-Rehner constitutive equation does not apply in a meaningful way, since, for example, it is not possible to define (and to measure) a Flory interaction parameter if no solvent is present. For this reason, a classical Fickian diffusion is instead assumed:

$$\frac{\partial C}{\partial t} = D_{02} \frac{\partial^2 C}{\partial X^2} \tag{3.27}$$

To solve Eqq. 3.25-3.27, boundary conditions are needed. As already mentioned, equilibrium condition is assumed at the interface between water and the hydrated polymer $X = 0$, while at $X = +\infty$ the film will be considered dry at any time. Moreover, a concentration C_h is attained at the hydration front $X = X_h$. The boundary conditions to be applied are thus:

$$\begin{cases} C(X=0, t \geq 0) = C_\infty \\ C(X = X_h(t), t \geq 0) = C_h \end{cases} \tag{3.28}$$

for the hydrated side, and:

$$\begin{cases} C(X = X_h(t), t \geq 0) = C_h \\ C(X = +\infty, t \geq 0) = 0 \end{cases} \tag{3.29}$$

in the dry side. At this stage, the concentration on the hydration front C_h is still unknown. However, in the next section it will shown how C_h can be determined, because of the requirement to fulfill for the mass balance across the interface:

$$D_{01}\xi(C_h)\frac{\partial C}{\partial X}\bigg|_{X=X_h^-} = D_{02}\frac{\partial C}{\partial X}\bigg|_{X=X_h^+} \tag{3.30}$$

ODE Formulation

Eqq. 3.25-3.27 and boundary conditions 3.28-3.29 can be rewritten in a still more convenient way, expressing the concentration not as a function of X and t, but as a function of a single independent variable.

By defining:

$$\eta = \frac{X}{\sqrt{D_{01}t}} \tag{3.31}$$

the problem can be indeed expressed as a system of independent Ordinary Differential Equations (ODEs), and not as two Partial Differential Equations (PDEs), as it will be seen in a moment.

Using the chain rule for the partial derivatives, Eqq. 3.25-3.27 become, respectively:

$$\begin{cases} \frac{d^2C}{d\eta^2} = -\frac{1}{2\xi(C)}\eta\frac{dC}{d\eta} - \frac{\xi'(C)}{\xi(C)}\left(\frac{dC}{d\eta}\right)^2 \\ \frac{d^2C}{d\eta^2} = -\frac{D_{01}}{D_{02}}\eta\frac{dC}{d\eta} \end{cases} \tag{3.32}$$

where $\xi(C)$ is given by eq. 3.26 and $\xi'(C) = \frac{d\xi}{dC}$. Concerning the boundary conditions, Eqq. 3.28-3.29, transform into:

$$\begin{cases} C(\eta = 0, t \geq 0) = C_\infty \\ C(\eta = \eta_h(t) = \frac{X_h(t)}{\sqrt{D_{01}t}}, t \geq 0) = C_h \end{cases} \tag{3.33}$$

and

$$\begin{cases} C(\eta = \eta_h(t), t \geq 0) = C_h \\ C(\eta = +\infty, t \geq 0) = 0 \end{cases} \tag{3.34}$$

respectively.

In the general case, the coordinate η_h indicating the hydration front is a function of time. It is, as a matter of fact, the only place in this problem formulation where time explicitly shows on.

It is here emphasized, however, that $\eta_h(t)$ is still unknown, because of its definition in terms of $X_h(t)$, which itself is presently unknown. Here comes the working hypothesis in the model, whereby the numerical value of $X_h(t)$ is always taken to be equal to the numerical value of $x_h(t)$, namely:

$$\forall t \quad X_h(t) = x_h(t) \tag{3.35}$$

and $x_h(t)$ is considered as a known input in the problem (as previously mentioned, this front is measurable, at least in principle, in the lab-fixed frame). Of course, eq. 3.22 will also be affected by this hypothesis. It is worthly emphasizing that eq. 3.35 is always assumed to hold in previous modelling papers for absorption and swelling, and that its status as a working hypothesis is often barely recognized, as discussed in the Conclusions of this work.

With 3.35 enforced, the mathematics becomes as follows. Once a time where the solution has to be calculated is given, η_h becomes a known scalar (since the front position $X_h(t) = x_h(t)$ is a given input). The algorithm can thus proceed as follows:

1) The time where the solution has to be calculated is chosen, thus assigning a value to η_h;

2) A tentative value for the concentration C_h at the hydration front is assigned;

3) Equations 3.32 are solved together with boundary conditions 3.33-3.34 by means of shooting method (*solve_ ivp* routine from the Scipy package [78] has been used in this work).

Once Steps 1-3 are completed, one has to check if mass balance is fulfilled across the hydration interface, by checking if condition

$$D_{01}\xi(C_h)\left.\frac{\partial C}{\partial \eta}\right|_{\eta=\eta_h^-} = D_{02}\left.\frac{\partial C}{\partial \eta}\right|_{\eta=\eta_h^+} \tag{3.36}$$

which stems directly from eq. 3.30, is respected. If this is not the case, another value of C_h has to be assigned, until convergence of the algorithm within a certain tolerance is attained. The concentration profile has thus been found at the given time. The procedure is repeated again with different times.

Formulating the problem in terms of a single independent variable η is thus making any time independent from the others, so one is able to solve the equations directly at a desired time, without knowing the concentration evolution.

In other words, there is no need of having an explicit function $X_h(t)$ describing the position of the solvent front as a function of time: as long as the front position is experimentally accessible at a given time, the concentration profile can be directly calculated at that time.

However, in order to have cleaner results, in the following section the hydration front is assumed to be well described by a power-law function:

$$x_h(t) = k_h t^\alpha \tag{3.37}$$

Under this hypothesis, the solution of the equations 3.32 with boundary conditions 3.33-3.34 requires the knowledge of 5 parameters:

- N, the number of sub-chains per unit volume;
- χ, the polymer-solvent interaction parameter;
- $D_{01} = D_1(C_\infty)$, the water diffusion coefficient on the swelling front;
- M, the positive constant describing how diffusion coefficient changes in the hydrated side: $D_1 = D_{01}e^{M\nu(C-C_\infty)}$;
- D_{02}, the water diffusion coefficient in the dry side of the film.

In principle, all of these parameters can be accessible from separate independent experiments. Once the parameters are estimated, the entire concentration profile $C = C(\eta) = C(X,t)$ is accessible. From this information, the position of the swelling front as a function of time can be calculated by (the modified) eq. 3.22, thus predicting the volume increase of the film.

Finally, measuring the volume increase implies measuring also the absorbed solvent mass m_s: since volume additivity is assumed, indeed, the increase in film volume is entirely ascribed to water accomodation. The swelling and the mass of absorbed solvent are thus related by the (constant) solvent density ρ_s:

$$m_s = \rho_s x_s \tag{3.38}$$

3.2 Model Applications

This section will show how the model developed in the previous section is applied to predict the absorption and swelling behaviour in three different systems: water in a chitosan-based polymer film [8], methanol in Polymethyl methacrylate (PMMA) [31, 12], and water in PVA. The data of the first two systems were published in literature; the last system has been experimentally analyzed in this work (see Chapter 4).

3.2.1 Case I Diffusion

Diffusion of liquid water in a chitosan film showed a Case I diffusion behaviour [8]. Due to the aforementioned similarities between the theory developed in ref. [8] and the model described in the previous section, all the parameters needed for the solution of the equations are directly available in [8] and are here reported in Table 3.1. It is worth noting that the diffusion coefficient in the hydrated side is considered to be a constant, thus $M = 0$.

With these values, Eqq. 3.32 could be implemented together with boundary conditions 3.33-3.34. Since in Case I diffusion $\alpha = 0.5$, η_h in the second condition of eqq. 3.33 becomes a constant, independent from time:

$$\eta_h = \frac{k_h}{\sqrt{D_{01}}} \tag{3.39}$$

and thus the solutions are self-similar when C is plotted against η. The iterative procedure illustrated in Section "ODE Formulation" is thus not needed in this case, and the system of equations has to be solved just once. The results are reported in Fig. 3.3 as νC vs X: in this coordinate, obviously, the solution will be parametric in time, since self-similarity is lost. The right panel of this figure represents the comparison between our model and the prediction by Mao et al. [8]. 5 different times are plotted in the range $[0 - 1800]\ s$. Notice that in this interval the water front has not yet reached the end of the slab, i.e. the process is still in the so-called coupled hydration and diffusion state.

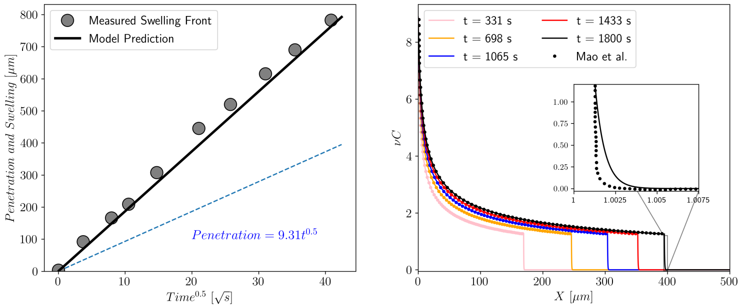

Figure 3.3. Model results for the system water-chitosan. Prediction for film thickness and comparison with the experiments are presented in left panel. Predicted concentration and comparison with Mao model are on right panel: solid lines represent the output of our model, points are the concentration as predicted by Mao et al. [8].

Is it clearly visible that the two models give the exact same concentration in the hydrated side. The inset shows instead the differences for the dry side of the polymer matrix. Interestingly, despite these differences, the concentration C_h that guarantees the mass conservation across the hydration front is the same. In the left panel the model prediction for swelling is shown as a function of $t^{0.5}$. It is represented by a straight line, confirming the Case I diffusion behaviour, and fits the experimental data quite well.

3.2.2 Case II Diffusion

The model chosen as an example of Case II diffusion is liquid methanol in PMMA, the one studied in the seminal paper by Thomas and Windle

[12], that still gains a lot of interest nowadays [79]. Penetration front and swelling as functions of time were experimentally obtained in Ref. [31]. Penetration front as a function of time has been fitted with a linear function, obtaining $k_h = 1.8 \cdot 10^{-9} m/s$ and, obviously, $\alpha = 1$. Swelling front x_s was not directly shown in [31]; however, the distance between the water-hydrated film interface and the hydrated-dry interface is given at any time: subtracting the penetration distance by this quantity x_s is obtained.

Notice that in this experiment, as opposed to the previous case of the chitosan-water system, the difference between D_{01} and D_{02} is less marked. Thomas and Windle propose as reasonable values $D_{02} = 10^{-14} m^2/s$ and $D_{01} = 5 \cdot 10^{-12} m^2/s$, assuming that the diffusion coefficient continuously increases exponentially with solvent concentration throughout the entire slab $D = D_{02} e^{23\nu C}$ (and it is $D(C_\infty) = D_{02} e^{23\nu C_\infty} = D_{01}$) [46] (no discontinuity is assumed at the hydration front). In the implementation of our model, it is assumed that in the dry side the diffusion coefficient is constantly D_{02}, while the same exponential law has been kept in the hydrated side.

All the other values are explicitly given, or can be easily calculated, from the references [31, 12] and are listed in Table 3.2.

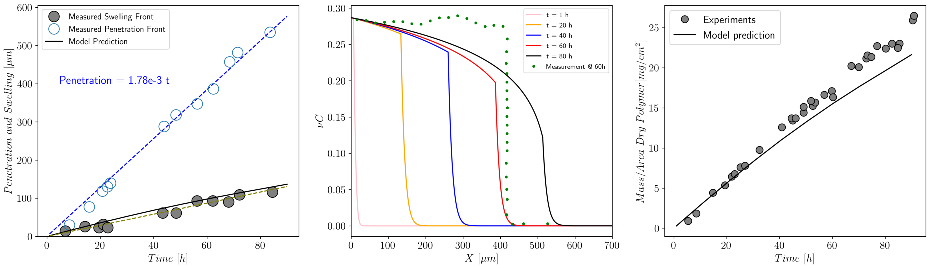

Figure 3.4. Model results for the system methanol-PMMA with $M = 23$ (as estimated by Thomas and Windle [12]). Left panel shows experiments and predictions on penetration and swelling: empty circles represent experimental penetration data, while full circles are positions of the swelling front; dashed lines are linear fits, while the solid black line is the model prediction. Central panel shows, in solid lines, the concentration predicted by our model at 5 different times, while points represent measurements at 60 hours. Right panel shows measurements of solvent mass in full circles and model prediction with a solid line.

Fig. 3.4 shows model predictions for swelling (obtained via eq. 3.22, and shown in left panel), concentration (central panel), and absorbed mass (right panel) and the respective experimental results. Notice that to obtain mass predictions, eq. 3.38 has been multiplied by a factor 2, since in the experiment by Thomas and Windle swelling occurs on both sides of the slab, that it is completely immersed in methanol. Data prediction is not perfect, especially for concentration and mass predictions. To reduce the gap between model and experiments, M has been changed: this is not a problem since, as Thomas and Windle state "These values [for the diffusion coefficient] are chosen as being both typical and reasonable; however, considerable uncertainty must remain". Our best fit is obtained with a value of $M = 28$ and the results are shown in Fig. 3.5. Agreement is excellent.

Notice that, in this system with a glassy polymer film, it was impossible to predict diffusion behaviour with a constant diffusion coefficient, as instead was done for Case I diffusion (see previous section).

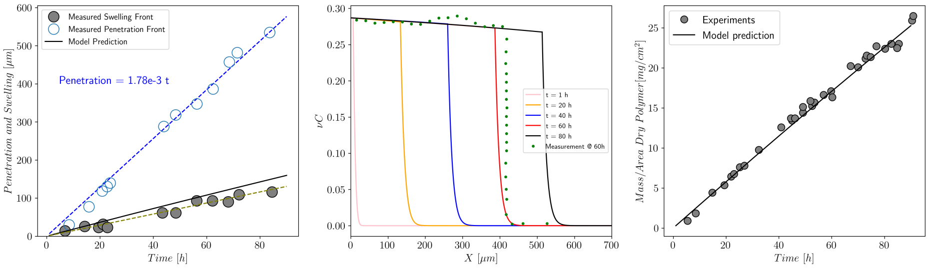

Figure 3.5. Model results for the system methanol-PMMA with $M = 28$. Left panel shows experiments and predictions on penetration and swelling: empty circles represent experimental penetration data, while full circles are positions of the swelling front; dashed lines are linear fits, while the solid black line is the model prediction. Central panel shows, in solid lines, the concentration predicted by our model at 5 different times, while points represent measurements at 60 hours. Right panel shows measurements of solvent mass in full circles and model prediction with a solid line.

3.2.3 Anomalous Diffusion

The model is here also applied to a system of PVA-water that showed anomalous diffusion, with the best power-law fits for penetration and swelling having an exponent included in the interval $]0.5 - 0.8[$. The description of this system and of the methods to estimate all the needed parameters will be given in Chapters 4-5. Figure 3.6, however, anticipates some results, showing the excellent agreement between the model prediction and the experimental data, regarding both the swelling front and the absorbed mass. It is interesting to notice that for Case I diffusion C_h is a constant, while for Case II and anomalous behaviours C_h decreases in time.

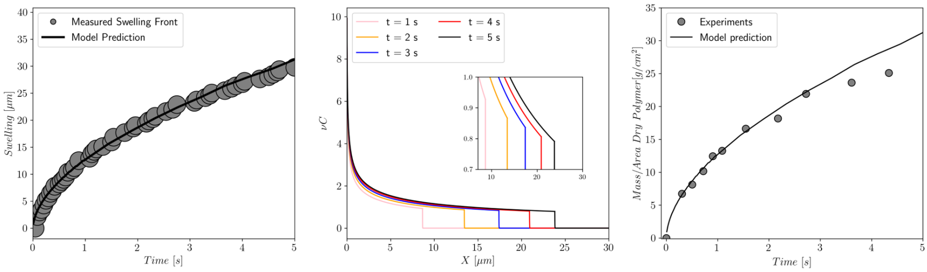

Figure 3.6. Model results for system water-PVA. Left panel shows measured swelling front (circles) with the model prediction (solid black line); central panel shows the concentration profile for 5 different times; right panel shows measured absorbed mass (circles) with the model prediction (solid black line).

Table 3.1. Parameters used in system chitosan-water

Parameter	Value
D_{01}	$5.15 \cdot 10^{-9} m^2/s$
D_{02}	$5.15 \cdot 10^{-14} m^2/s$
M	0
χ	0.41
N	$4.25e^{24} m^{-3}$
ν	$3 \cdot 10^{-29} m^3$
k_h	$9.31 \cdot 10^{-6} m/\sqrt{s}$
α	0.5

Table 3.2. Parameters used in system PMMA-ethanol

Parameter	Value
D_{01}	$5.15 \cdot 10^{-9} m^2/s$
D_{02}	$10^{-14} m^2/s$
M	23
χ	1
N	$3.5e^{27} m^{-3}$
ν	$6.72 \cdot 10^{-29} m^3$
k_h	$1.8 \cdot 10^{-9} m/s$
α	1

CHAPTER 4

Materials and Methods

In the first section of this Chapter, the polymeric films used in this work are presented. The second section describes instead the experimental techniques employed to study diffusion of a liquid solvent in polymeric films (subsections 4.2.1 and 4.2.2) and adhesion between two polymer layers (subsection 4.2.3).

4.1 Materials

4.1.1 Polymeric film

In this work, two polymeric films provided by Procter and Gamble (P&G), and mainly composed of Polyvinyl-alcohol (PVA), are studied. The other components and the exact differences in chemical formulations are not known in detail, since these materials are not produced in-house by P&G but commissioned to an external supplier. For this reason, and also to respect the confidentiality agreement, production names of these films are not mentioned; film A and film B are instead used to refer to them. Some results will be also shown for film A after an aging treatment, that consists in keeping the film in a room with a controlled temperature of 50

$^{\circ}C$ for one week. The two films, A and B, are used for different purposes: film A, indeed, is the one on which water is directly applied, while film B encounters the solvent only indirectly, when it is put in contact with film A.

PVA is an hydrophilic, synthetic polymer widely used for several industrial applications: due to its non-toxicity and bio-compatibility, for example, it has found large employment in pharmaceutical industry (drug delivery, ophthalmic formulations) [80, 81]. PVA is also used in food packaging [82], for its good barrier properties when cast into a film, and for tissue regeneration, thanks to its ability to form hydrogels [83, 84, 85, 86]. PVA seems thus a very good candidate for our scope: due to its hydrophilicity, in fact, water can be used to enhance chain diffusivity and promote welding between polymer layers; at the same time, it is very effective in protecting the final product from the surrounding environment.

4.2 Methods

4.2.1 Measurements of Penetration and Swelling

Water diffusion in PVA films is observed and analyzed by means of Optical Microscopy and Optical Coherence Tomography (OCT). Both techniques showed that water propagation occurs with the appearance of a sharp front beyond which the film is essentially dry, as often found in hydration of polymeric films, and as already discussed in Chapter 2. Such discontinuity has been named *penetration front* or *hydration front*. The other front introduced in Chapter 2, namely the *swelling front*, representing the increase in volume due to water accommodation, is also clearly visible. With both techniques, the position of these two fronts is tracked as a function of time by means of image analysis, using standard algorithms for edge detection: subsequent application of Median blurring and Sobel filter is sufficient to reliably detect the edges in both films. Image analysis has been performed in Python, mainly using OpenCV library [87]: *medianBlur* (with kernel size of 3) and *Sobel* (kernel size $= 7$) routines constitute the core of the developed tracking algorithm.

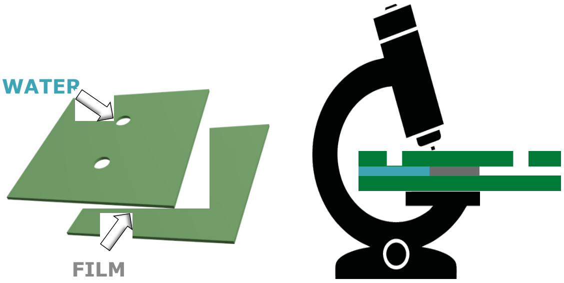

Figure 4.1. 3D representation and 2D section for Optical Microscopy setup.

Optical Microscopy

For our purposes, any standard microscope is suitable: in this study, a Leica LSP DM with a magnification of 2.5x was used (spatial resolution: 2.2 μm). A small (length 1 cm x width 1 cm, thickness 76 μm) piece of PVA film is sandwiched between two Perspex plates (5 cm x 5 cm), held together by magnets to ensure a constant pressure throughout the measurements. This setup is inspired to a similar one used by Petropoulos and Sanopoulou [28, 26], with the magnets substituting the clamps. The bottom slide is the one on which PVA sample lays, while the top one is pierced to allow water application. Once the film is positioned in between the slides, the microscope is focused (top view) on the interface between the sample and the air, and recording is started. 15 ml of water are applied through a simple pipette and 10 s of diffusion are recorded at 24 fps. 5 repetitions are performed on each film. It is worth noting that higher quantities of water led to the same results (indicating that 15 ml of solvent are enough to saturate the film absorbing capacity).

Bright field has been preferred over polarized light. The latter, indeed, enhances the contrast between isotropic and anisotropic media, facilitating the recognition of the penetration front, but at the same time makes the swelling front more difficult to track. This is especially true at longer times, when the content of water throughout the film increases.

With this setup, optical microscopy turned out to be a very reliable and cheap method to observe liquid solvent absorption and swelling of the polymeric films, making it possible to measure the time dependence of both penetration and swelling fronts' positions at the same time. However, this methodology has strong limitations. First: in this arrangement, water is diffusing along the width of the film. The conditions of this experiment are thus somehow different from what happens in several applications, including the solvent-sealing of polymer layers, where solvent is applied on top of the film surface and diffusion occurs along the depth of the matrix [8]. Second: it is not possible with Optical Microscopy to extract information on concentration profiles in the slab. Thus, although having available (Chapter 3) a model capable to predict solvent quantity in the film as a function of time and space, such a detailed information is not accessible experimentally with this technique: model validation will thus be carried on only through the position of the swelling front.

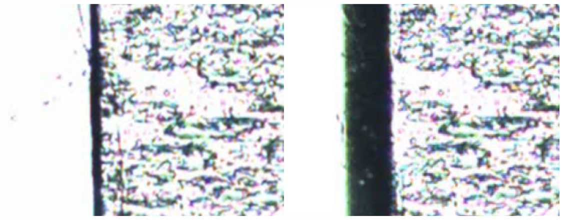

Figure 4.2. Snapshot of Optical Microscopy video recording before (left) and after (right) contact with water. The thin black line on the left panel is the interface between air and the film; the large black stripe on the right panel fully encompasses the hydrated region.

Optical Coherence Tomography

To overcome the limitations of optical microscopy, thus allowing for observing the diffusion throughout the depth of the film, Optical Coherence Tomography (OCT) is employed.

OCT is a non-destructive imaging technique widely used for medical purposes, like dermatology [89] and ophthalmology [90]; recently, its usage has been extended to a broad range of non-medical applications [91], including optical analysis of various film properties [88]. It is capable to provide cross-sectional and three dimensional reconstructions of an object, based on transmission and scattering of a low-coherence light source. OCT is often compared to ultrasound, due to their similar working principles [92]: waves (sound or light) are directed through the sample, and the

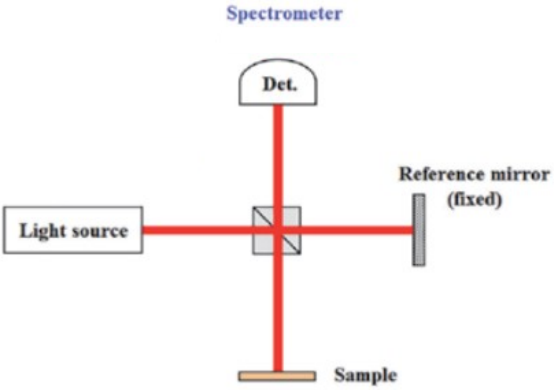

Figure 4.3. Basic scheme for the functioning of OCT. Adapted from [88].

return time for the back-scattered wave is measured, giving information on shape, morphology and possible flaws in the specimen. Return time of the light beam cannot be measured directly: OCT is in fact an interferometric measure. Source light is splitted into two parts: one goes to the sample and the other to a reference arm of known length (usually a mirror). Since the light source is broadband, the reconciling of the two returning light beams creates an interference pattern, from which the light intensity can be obtained as a function of z, the sample depth direction: this is the so-called A-scan. Multiple A-scans can be assembled together to create a B-scan (Brightness scan), the cross-sectional image of the sample.

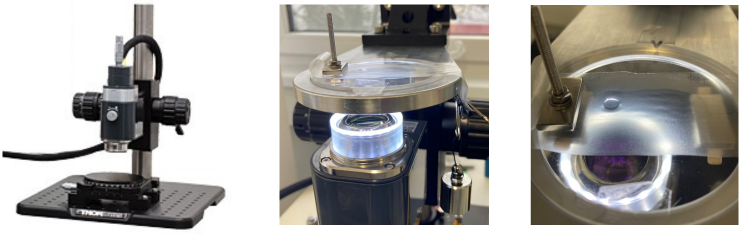

Figure 4.4. Basic (left) and modified (center and right) setup for OCT. Central and right images show how the PVA film is kept in place by magnets and the application of a water droplet.

The apparatus employed in this work is available in P&G facilities in Frankfurt (DE). It is a custom version of Ganymede^{TM} Series by ThorLabs, an OCT instrument with a center wavelength of 900 nm and an high axial resolution of 1.2 μm. To the basic setup, an acrylic glass plate with magnet bars is added for the sample positioning (Fig. 4.4). This plate is covered with a thin layer of silicon oil to improve image quality, reducing noise; the PVA film is thus placed on the plate and kept in position with magnets, or with magnets and a weight like in Fig. 4.4, to avoid wrinkles and other instabilities that can appear during water diffusion. A droplet of 10 μl of water is added on the film surface with a pipette and the diffusion process is recorded for 10 s. During this time, 5 B-scans are taken: in this way, a smooth 2D gray-scale image that reconstructs the specimen along z-axis is obtained from the average over the 5 different B-scans. To be sure that film is saturated in the analyzed time span, water content was increased up to 1 ml without any noticeable difference in the absorption process. Notice that the required quantity of water is much smaller as compared to the one needed for the optical microscopy experiment: this is due to the reduced area over which the solvent is spread in this case. As already mentioned, 5 B-scans are performed on each sample. Moreover, 5 different samples of each film are examined.

In measuring swelling and penetration distance fronts with OCT, the refractive index of the film was considered to be constant: this hypothesis is made to maintain the same scaling between optical and physical dimensions throughout the entire test. In general, refractive index of the medium should instead change, decreasing with the increase in water content. The refractive index of dry PVA, in fact, has been estimated by means of 3D Ellipsometry in P&G Mason (Ohio) facilities to be $n_{PVA} = 1.58$, while the one of pure water is $n_{H2O} = 1.33$. With the hypothesis of a linear dependence in refractive index of the medium n_{group} on the volume fraction of the two components ν_{H2O}, ν_{PVA}:

$$n_{group} = \nu_{H2O} n_{H2O} + (1 - \nu_{H2O}) n_{PVA} \tag{4.1}$$

The relative error

$$E_r = \frac{n_{PVA} - n_{group}}{n_{PVA}} \tag{4.2}$$

is estimated to be around 8% when water volume fraction reaches a value of 0.5. It is also worth noting that the maximum relative error, i.e. when $n_{group} = n_{H2O}$ would be of about 16%. This error is considered to be negligible, and the hypothesis of a constant refractive index is kept.

As a final note, OCT could also overcome the impossibility to measure the entire water concentration profile (a limitation of Optical Microscopy already mentioned in the previous subsection, where the color differences in the hydrated region are less marked): with an appropriate calibration curve, in fact, it could be possible to directly correlate the pixel color intensity of in the gray scale to the local solvent content. In this work, however, such a calibration curve is not created and OCT is employed to only measure the positions of swelling and penetration fronts as functions of time.

The possibility of measuring the complete concentration profile via OCT is a future perspective of this work.

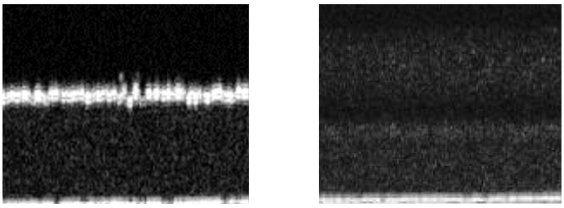

Figure 4.5. Snapshots of OCT B-scan reconstruction before (left) and after (right) contact with water.

4.2.2 Sealing Test Stand

Sealing Test Stand (STS) is a machine commissioned by the P&G facilities in Bruxelles and built with the specific purpose of studying the solvent-assisted welding of polymeric films. In this work, it has been used for two different tests: the measurement of the maximum mass of water the film can absorb as a function of the diffusion time (absorption curves) and the evaluation of the seal strength between two films. A schematization of STS, with the two different configurations for the two experiments, is given in Fig.4.6.

Two rolls of film (the big circles 1 and 2 in the picture) are put on two unwinders in the machine. It is here recalled that film A (placed on

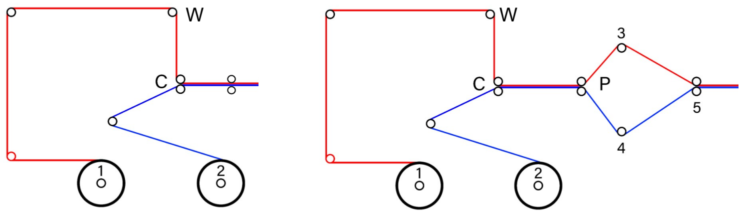

Figure 4.6. Sealing Test Stand schematization. Left image represents the configuration for the absorption curve test; right image is the setup to measure the peel force.

unwinder 1) is the one that is directly wetted, while film B (on unwinder 2) encounters the water only indirectly, by contact with film A. In this schematics, film A is represented by a red line, and is wetted in point W; film B is the blue one, and the two are put in contact in point C. From point C on out, the setup of the machine changes depending on the desired test.

To measure the peel force, the two films are peeled apart in point P, where two loads cells (circles 3 and 4) measure the force needed to break the seal; in this case, in point 5 the two films are put in contact again to make it easier the exit from the machine. Notice that, in points 3-4, also some additional peel rollers, with adjustable speed, are present; to simplify the schematics, however, they have not been drawn.

If, instead, the aim is to create an absorption curve for the film, the bond is not broken in point P, the material directly exits from the machine and is weighted separately, as discussed below.

Notice that, in both scenarios, the described process works in continuous, with the unwinders that keep rotating, unfolding the film that enters in the machine with a desired speed. The adjustable parameters on STS are:

- Coat Weight, the mass of water to apply per unit area on the film $[g/m^2]$;
- Line Speed $[m/s]$;
- Open Distance, the space from application point to combining point (WC Distance) $[m]$;

- Curing Distance, the space from combining point to peeling (CP Distance);
- Pressure applied at the combining point C [bar];
- Speed of peel rollers in 3-4, that can rotate with a velocity independent from the line speed [m/s].

Absorption Curves

In this section the protocol to create absorption curves is described. The aim is thus to measure the maximum mass of water the film can absorb as a function of the *Open Time*, defined as:

$$Open\ Time = \frac{Open\ Distance}{Line\ Speed} \tag{4.3}$$

To estimate the quantity of solvent the film can absorb, the used setup is depicted in left panel of Fig.4.6, where the two polymer layers are not separated and directly dragged outside from the machine.

Once the two films start to exit the STS, an operator proceeds to cut and weight on a scale 1.5 m of film, repeating the task 5 times to minimize human error and random variability inside the film rolls. The procedure has to be repeated without applying water, to have a dry baseline for the film mass: the difference between the masses of wet and dry films gives a gravimetric estimation of the grams of solvent absorbed.

To be sure that the size of film sample is constant throughout the measurements, the last roll of STS has been equipped with a metal plate that marks down the film every time it completes a full round. Due to film wrinkling when wet, in fact, it is quite difficult to measure exactly 1.5 m of film each repetition; the marks on the films, at a fixed and known distance, help to always weight the same amount of material, leading to a huge decrease in standard deviation of this test method.

It is essential, of course, to choose a quantity of water sufficient to saturate the *instantaneous* absorption capacity of the film, simulating a thermodynamic bath. To reach this purpose it is possible on STS, as mentioned, to change the applied Coat Weight to a desired target value: the coat weight can thus be increased step by step until the presence of

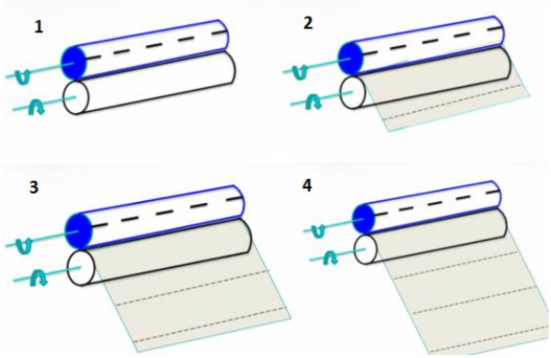

Figure 4.7. Representation of the two final rolls in STS. As time goes on, film exits from the machine with marks (dashed lines) imprinted by the metal plate.

free water, not yet absorbed by the film, is visually observed. In this way the absorption capacity of the material is not underestimated. Notice, however, that also the weight free water on the film surface would be measured on the scale, since it would be absorbed by the dry film. It is essential, in this regard, to increase the Coat Weight up to the minimum value in which free water appears and perform the measurement at that value.

The procedure just described leads to the measurement of a single point in the absorption curve: the 5 repetitions are indeed taken at same line speed and same WC Distance, i.e. the same Open Time. Since the entire dependence of absorbed mass on time is desired, the procedure has to be repeated several times changing, for example, the WC Distance and keeping the line speed constant: in this way the time given to the water to diffuse inside the film is modified and for every distance a point in the graph mass absorbed vs time is created. In our case, on changing the Open Distance and the Line Speed in the range permitted by the machine specifications, the absorbed mass can be measured in an interval of $[0.3-5]$ seconds.

Measurements of peel force

As mentioned in the previous subsection, the STS is also capable to peel the two films welded together and to measure the force needed through two load cells (setup in right panel of Fig.4.6). A test method has been developed and some preliminary experiments for measuring the seal strength have been performed.

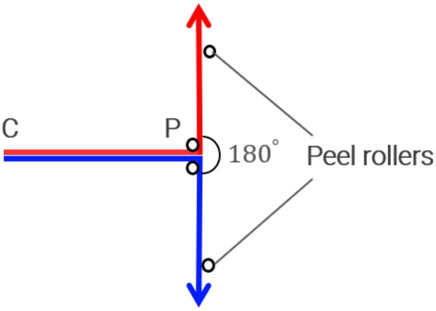

Figure 4.8. Idealized condition of the peeling mechanism.

To schematize the force balance holding in the system, ideal conditions are here assumed: load cells are thus considered pulleys with negligible mass and diameter, and the film splitting happens with a 180 degrees angle (Fig. 4.8). In this situation, only three forces play a role: the tension read by the load cells, F_{LC}, the actual peel force, F_P, and the force due to stretching in the peeling arms between peel point P and peel rollers 3-4, F_S. The force balance reads:

$$F_{LC} = F_P + F_S \tag{4.4}$$

It is thus clear that, in order to measure through the load cells the peel force only, the stretching contribution in the peeling arm must be negligible. In STS, the film stretching after the peel point can be modified on changing the velocity of the peel rollers: the faster the peel rollers rotate compared to the line speed the more the material is elongated. Thus, ideally, the test should be performed with the speed of peel rollers being equal to the line speed. In such a configuration, however, STS is not able to break the joint: the film thus continuously enters in the curing distance (segment CP) and the machine is not able to pull it outside with a sufficient speed. This material accumulation will thus lead to the formation of waves in the curing distance (see left panel in Fig. 4.9). The presence of waves is undesirable, since measurements become unreliable, with the STS eventually stopping after few seconds. Instead, in order to have a straight film in the curing distance, the speed of the peel rollers is increased step by step, up to the point where the measurement is stable and no waves appear (right panel in Fig. 4.9). In this *minimum* working condition, the stretching contribution is considered negligible and the force measured by the load cells is F_P. Notice that increasing the speed of the peel rollers further would lead to an additional contribution to the measured force, due to film stretching. A force measurement is considered to be reliable when the test runs stable without waves for at least one minute; 3 repetitions are performed in the same conditions to check test repeatability. The sum of forces measured by the upper and the lower load cells is taken as a proxy of peel strength.

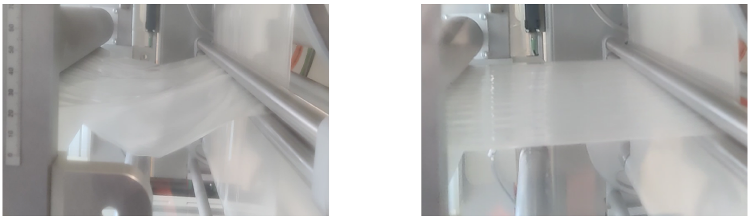

Figure 4.9. Peel measurements with (left panel) and without (right panel) waves formation. Right image represents the condition where measurements of peel force are reliable.

CHAPTER 5

Experimental and modelling results

This Chapter is divided into two sections. The first one presents experimental results on water diffusion (i.e., penetration and swelling fronts tracking and absorption curves) and on layer to layer adhesion (peel tests) for different films; the second one describes how the model presented in Chapter 3 has been applied to our system PVA-water and how effective it is to describe absorption and swelling processes taking place in the polymeric film.

5.1 Experimental Results

5.1.1 Penetration Distance and Swelling

Optical Microscopy

In Fig. 5.1 three frames of a typical recorded video are shown. At time zero, left image, there is no water and the focus of the image is at the interface between the film and the air. Some structures are clearly visible in such top view of the polymer matrix. The central panel shows the situation after 5s from water application. In this image, water diffuses going from left to right. Two sharp fronts have appeared: the one on the right, indicated by a light blue line, is the penetration front; the one on the left, instead, is the 1D swelling front. At short times, swelling front travels faster than the penetration front; at longer times, however, a plateau is observed for the swelling front, while water keeps entering in the polymer. Comparison between the second and third (10s from water application) panel of Fig. 5.1 makes this behaviour clearly visible. In both these images, in fact, light blue and grey lines represent, respectively, penetration and swelling fronts at the time of the *central* frame, while the red line is the original air-film interface: going from 5 to 10 s, swelling front has remained essentially in the same position, while penetration front kept moving.

This phenomenon can reasonable be explained as follows:

- The water content near the swelling front becomes so high that the swollen area of the film becomes essentially indistinguishable (within our accuracy) from the pure solvent;
- Dissolution has started. As already mentioned, in fact, PVA is a water-soluble material.

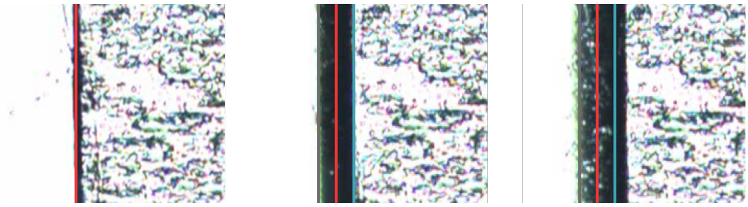

Figure 5.1. Three subsequent frames (dry film, hydrated film after 5s of diffusion, hydrated film after 10s of diffusion) extrapolated from a typical Optical Microscopy video. Red line represents the original interface air-polymer; light blue and grey lines represent, respectively, penetration and swelling fronts at the time of the central frame.

It should be highlighted, however, that the plateau in the curve swelling vs time occurs at longer times than the ones of interest for our main application, i.e. solvent-sealing for the production of laundry detergent pods: for this reason, this issue is not investigated further.

Penetration and swelling fronts can be plotted as functions of time. In all these graphs, the fronts' position is defined in a lab-fixed frame of reference with the zero positioned at the original air-polymer interface. Taking as example the central frame of Fig. 5.1, swelling front position will be defined as the distance between gray and red lines, while penetration front position will be defined as the distance between light blue and red lines.

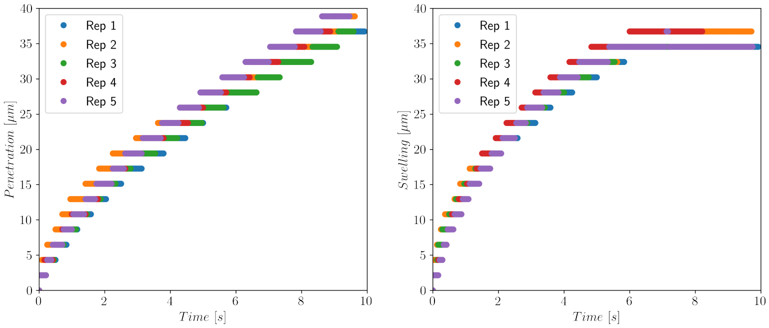

Figure 5.2. Penetration (left) and Swelling (right) as functions of time for film B. 5 different repetitions are presented.

In Fig. 5.2 penetration and swelling fronts measured in Film B are reported (5 repetitions). The peculiar shape made by "steps" is, of course, due to the space resolution of the microscope: the position of the fronts seems constant for a time span and then jumps to the next "step". In taking the average of the repetitions, however, only the first point of the step is considered as the true position of the front.

Reproducibility of the experiment is quite good, with a small standard deviation, especially at short times. The aforementioned plateau in the swelling front is observed starting from $6s$, while the penetration distance keeps increasing. It is here anticipated that the model presented in Chapter 3 cannot account for such a possibility, only giving strictly monotonic fronts; however, as already mentioned, for our target application only the first 5 seconds of diffusion are interesting and the plateau can be disregarded. In this time range, the average swelling and the average penetration are directly compared in Fig. 5.3. Dashed lines represent the best power-law fit at^b of the two quantities, with $a = 9.7 \pm 0.1, b = 0.63 \pm 0.01$ for penetration and $a = 13.6 \pm 0.1, b = 0.56 \pm 0.01$ for swelling (confidence

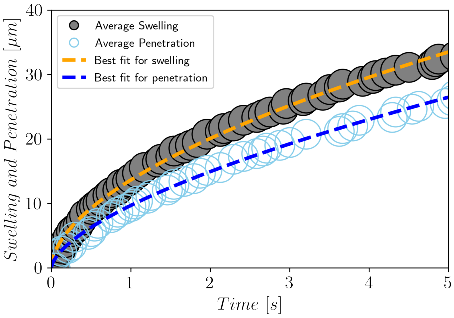

Figure 5.3. Average Penetration and Swelling as functions of time for film B. Dashed lines represent the best power law fits (see text) for the two sets of data.

level = 95%). Thus, as already mentioned in Chapter 3, diffusion in PVA-water system can be defined anomalous. Interestingly, fittings suggest that the two exponents of the power-laws are different from each other, with swelling being closer to a Case I Behaviour. Notice that for Case I and Case II Diffusion, as we saw in Chapters 2-3, the two power laws are instead equal.

Analogous results are shown for film A in Fig. 5.4, where penetration and swelling fronts are plotted as a function of time for 5 repetitions.

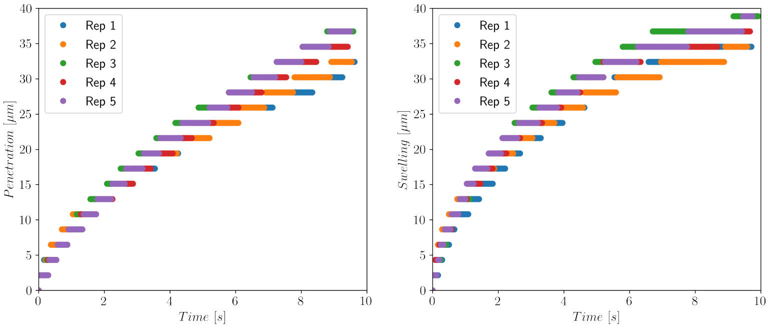

Figure 5.4. Penetration (left) and Swelling (right) as functions of time for film A. 5 different repetitions are presented.

The average behaviour of film A in the first 5 seconds is shown in Fig. 5.5. The best power-law fits obtained are $(8.5 \pm 0.1)t^{0.64\pm0.01}$ for penetration and $(12.6 \pm 0.1)t^{0.52\pm0.01}$ for swelling. Thus, also for this film, the two exponents are distinct, with the swelling being much closer to a Case I behaviour.

A direct comparison between the fitted behaviours of Film A and Film B is done in Fig. 5.6. Interestingly, diffusion in film B occurs with both a higher swelling degree and a faster solvent penetration: this probably happens since film B has only an indirect contact with water, and thus its higher hydrophilicity is needed to disentangle the polmymer chains, promoting a stronger joint.

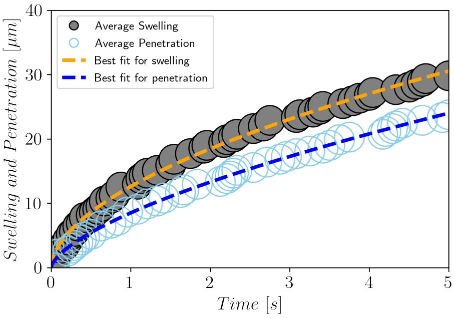

Figure 5.5. Average Penetration and Swelling as functions of time for film A. Dashed lines represent the best power law fits (see text) for the two sets of data.

To test the impact of the environmental conditions on water diffusion, the experiment is also repeated after Film A was aged for 1 week in a room with a controlled temperature of 50 $°C$. Fig. 5.7 shows the comparison between fresh and aged film, both in terms of penetration and swelling. It is really interesting to notice that swelling behaviour is exactly the same for treated and non-treated film, while penetration seems slower for the film that faced the aging process. As a perspective, it would be interesting to investigate the causes for this behaviour.

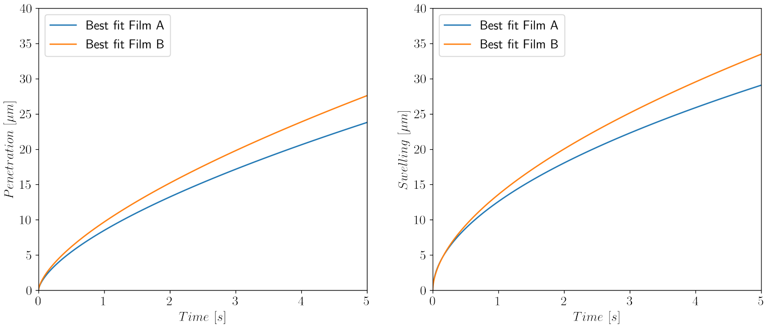

Figure 5.6. Measured Penetration (left) and Swelling (right) as functions of time for films A and B.

Optical Coherence Tomography

In this section, we show results from OCT measurements. For the sake of brevity, only results pertaining to film A are discussed, Fig.5.8 shows B-scan reconstructions of the diffusion and swelling process in three different moments: dry film before the diffusion starts (left image), hydrated film after $5s$ of diffusion (central image) and hydrated film after $10s$ of diffusion (right image). In the first image, the black area at the top is air, while the grey-sh (granular) medium in between the white line and the bottom of the image is the polymer film: white stripe, in fact, is the surface of the polymeric material, i.e. the location where the change in refractive index is bigger and the pixel intensity is maximum. When diffusion starts, water comes from top of the image (large black area previously occupied by air) and, like in Optical Microscopy, two sharp propagating fronts are observed, the swelling and the penetration, indicated by a sudden change in the refractive index of the medium. Below the lower front, the film is essentially dry, maintaining the same color pattern of the dry material in the left panel.

As for the case of optical microscopy, the initial interface air-film is marked by a red line. In the second and third frames, the gray line represents the position of swelling front at $5s$, while the light-blue one indicates the water penetration front at $5s$. In this way, it is immediately highlighted that, differently from Optical Microscopy, no (apparent) arrest

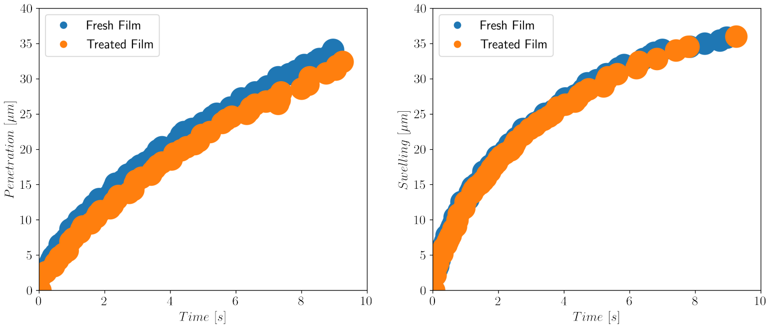

Figure 5.7. Comparison between average penetration and swelling for film A fresh and heat-treated (aged) at 50°C for one week.

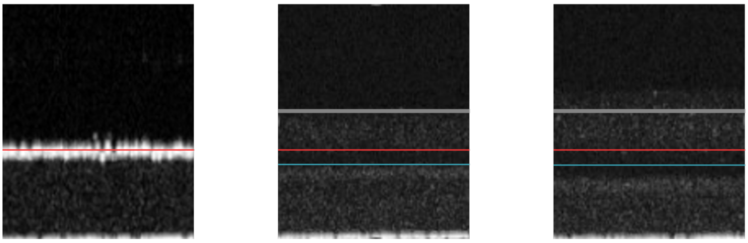

Figure 5.8. Three subsequent frames extrapolated from a typical OCT experiment: left (dry film), central (taken after 5s of diffusion), right (10s of diffusion).

of the swelling front is shown. This mismatch probably reveals the higher sensitivity of OCT technique to small differences in the local material properties: tomography can distinguish pure water from the hydrated film at any time in the observed range. A further cause of discrepancy could be the intrinsically anisotropy of diffusion in this medium, with different features depending on the direction in which water propagates. It should always be remembered, indeed, that water in OCT experiment propagates trough the film depth, while it propagates along the width of the film in the Optical Microscopy setup.

As a further observation, notice that for any time, the region in between the two fronts (i.e. the hydrated part of the film) is not entirely of the same color, but presents shades in the gray-scale that are more accentuated than in the case of Optical Microscopy: for this reason, as already mentioned, it could be possible to extract from OCT images the entire water concentration profile in the film. Notice, for example, that the area right above the penetration front is essentially black, like it is for the isotropic media (water and air): this could indicate a water concentration profile essentially constant above the hydration discontinuity (see the section 5.2 in this regard). The use of OCT to measure solvent concentration profile, however, would require the creation of a calibration curve to quantitatively (and not just qualitatively) link the pixel intensity to the local amount of water; this issue is not pursued in the present work.

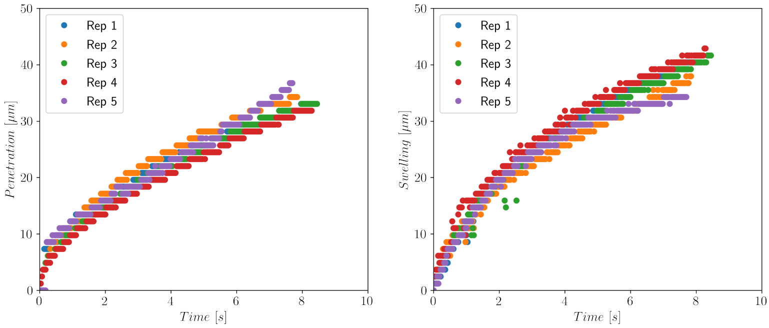

Figure 5.9. Penetration (left) and Swelling (right) as functions of time for film A, measured via OCT. 5 different repetitions are presented.

Measurements of the positions of swelling and penetration fronts for film A are shown in Fig. 5.9, for 5 different repetitions. Standard deviation among the different repetitions is quite small and the test method shows a good reproducibility. Is it visible that the measurements do not always reach 10s of diffusion: the reason is that even if the recorded experiment is of 10s, some time (usually a couple of seconds) is needed for the operator to drop the water on the film in the right spot.

Fig. 5.10 compares the results from Optical Microscopy and OCT for film A. Concerning penetration distance, the curves obtained from the two experiments are essentially equal; there is instead a difference in long time behaviour for swelling: as already discussed, OCT does not show a

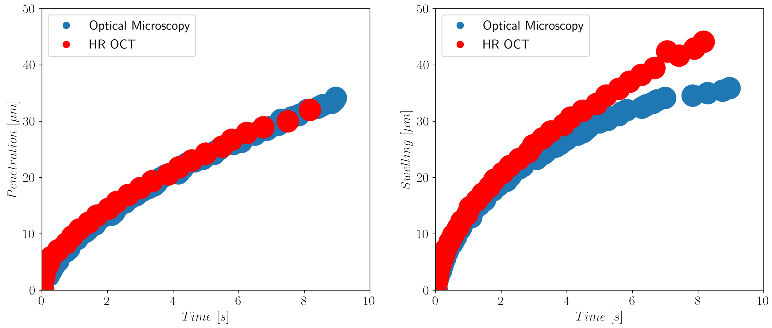

Figure 5.10. Average Penetration and Swelling as functions of time for film A. Orange points represent OCT experiments; blue points are results of Optical Microscopy experiments.

plateauing swelling front, like Optical Microscopy, and keeps increasing with a higher rate.

In Section 5.2, where the model developed in Chapter 3 is used to predict swelling behaviour for the system water-PVA, Optical Microscopy experiments are used for validation, since more data and a more reliable image analysis algorithm are available for this technique. However, the difference between the two experimental methods is negligible for the time-scale of $5s$ of diffusion.

5.1.2 Absorbed Mass

Absorbed mass as a function of time is plotted in Fig. 5.11 for Film A. For a direct comparison with Coat Weight, units are in g/m^2, since the weight of absorbed water has been divided by the area of film that absorbed the solvent. Points represent the average of the 5 repetitions, while the error bars indicate standard deviation. The best power-law fit obtained is $12.6t^{0.49}$, very close to the value of classical Fickian diffusion.

5.1.3 Peel Force

In Fig. 5.12 some preliminary results for peel tests are shown, using film A as the substrate that is directly wet, and film B as the dry one. Open

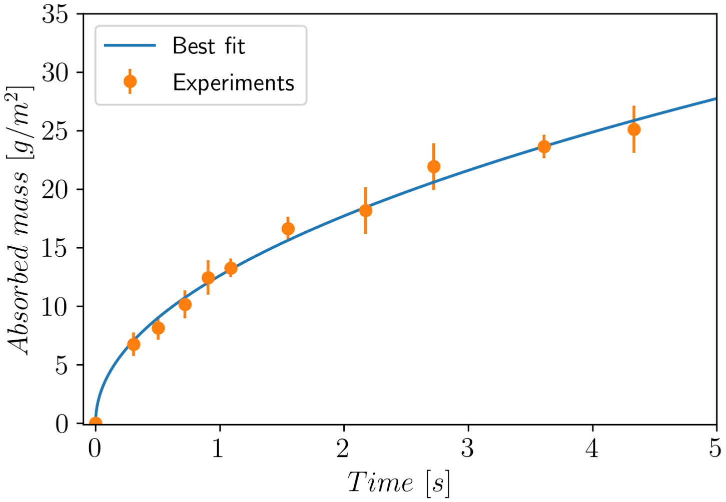

Figure 5.11. Absorbed mass per unit area as a function of time for film A. Points represent the average of 5 repetitions, while the errorbar is the standard deviation. Solid line represents the best obtained power-law fit: $M(t) = 12.6t^{0.49}$

time, Coat Weight and Curing Time are adjusted as to find operating conditions that lead to the maximum peel force. Forces are measured in the range [0.9-2.2] s of Open Time, for two different Curing Times (1.6 s on the left panel and 2 s on the right panel) and for Coat Weights of 6,7,8 or 9 g/m^2. As mentioned, only two values of curing time have been here investigated, which however are within the curing time window of the actual process, between 1 and 2 seconds. It is apparent that such time interval must be investigated in more detail, i.e., with a dense set of curing times. Notice also that this range of Coat Weights is well below the maximum absorbing capacity for film A (Fig. 5.11); however, increasing the Coat Weight made more difficult to obtain a reliable experiment that could match the criteria explained in the subsection 4.2.3 of previous Chapter. In the explored operating window, indeed, increasing the mass of water per unit area given to the film led to increasing the peel strength: for this reason, STS was not able to stretch the films enough to avoid waves formation. This is the reason why curves are not complete, with some missing points at the highest Coat Weights. Standard deviation is quite low, smaller than marker size.

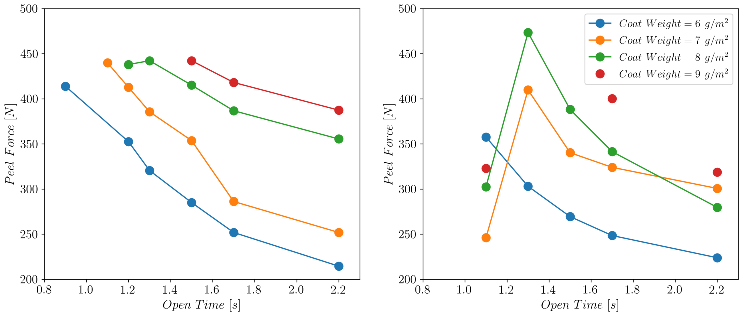

Figure 5.12. Peel force as a function of Open Time, parametric in Coat Weight. Two different Curing Times are shown: $1.6s$ in the left panel and $2s$ on the right panel.

For both Curing Times, it seems clear that Peel Force is increasing on increasing the Coat Weight.

The trend with Open Time, instead, is more complicated. When the Curing Time is equal to $2s$, in fact, a clear maximum appear in the curve Force vs Open Time, for every Coat Weight. These observations seem to indicate that, to obtain a good sealing, the water amount on the surface of the film is a key parameter: without enough water, or if we do not wait enough for it to penetrate inside the film, indeed, the peel force seems to be lower; on the other hand, if the open time is too long, water may progressively diffuse away from the interface, slowing down the disentanglement dynamics of the polymer chains, inhibiting the formation of a strong joint. Such a maximum is not present when Curing Time $= 1.6s$; however, Open Times shorter than $0.8s$ have still to be investigated.

Notice also that the impact of curing time is not as direct as one would expect for a dry sealing, as discussed in Chapter 2. Indeed, without solvents, the longer the curing time, the higher should the measured peel force be, increasing with curing time as:

$$P_f(t) \propto t^{1/4} \tag{5.1}$$

In our measurements, however, the trend of the force vs the curing time is not monotone at all, and it is highly dependent on the other operating conditions.

5.2 Modelling Results

In this section, the model developed in Chapter 3 and there applied to the systems chitosan-water and PMMA-methanol with data taken from literature, will be applied to the system PVA-water analyzed and described in Chapter 4. The first subsection illustrates how the parameters needed for the model implementation are estimated for Films A and B, while the second one shows the comparison, and excellent agreement, between predictions and experiments on swelling and absorbed mass for PVA films.

5.2.1 Parameters' estimate

Penetration front motion

The first parameter to introduce is the motion of the penetration front, i.e. the position of water front as a function of time. To estimate this, a fit of the penetration distance measured in optical microscopy has been done, giving, as already discussed and shown in Figg. 5.3-5.5, $8.5t^{0.64}$ for Film A and $9.7t^{0.63}$ for Film B. This directly returns the estimates of k_h and α for the two materials.

Polymer-solvent interaction parameter

For the polymer-solvent interaction parameter, the most common value measured in literature for the solutions of PVA in water at room temperature is here used : $\chi = 0.494$ [93, 94].

Volume of the solvent molecule

For the value of water molecule volume, $\nu = 3 \cdot 10^{-29} [m^3]$ has been chosen [8].

Diffusion coefficients

Since PVA is an highly hydrophilic material, the diffusivity in the hydrated part of the film has been chosen to be constant and equal to the self diffusion coefficient of water at $25°C$: $D_1 = D_{01} = D_{s.d.} = 2.3 \cdot 10^{-9} [m^2/s]$ [95].

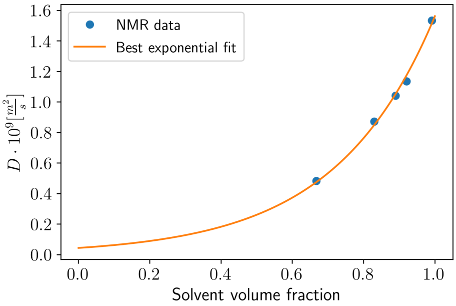

Figure 5.13. Measured Diffusion Coefficient of water by NMR in a solution of Water and PVA as a function of the solvent volume fraction. Solid lines represent the best exponential fit to the data.

As already discussed in Chapter 4, the exact chemical composition of the film is not known: thus, even if the main component is PVA, the affinity of our film with solvent could be somehow different compared to the pure material. To check the validity of choosing self-diffusivity as D_{01}, Fig. 5.13 shows 1H Nuclear Magnetic Resonance (NMR) measurements performed in the P&G facilities in Reading (UK). In the graph, measured diffusion coefficients are plotted as a function of the solvent volume fraction ϕ, at equilibrium, i.e., for the water-PVA solution. An exponential function with two free parameters $D = D_{dry} e^{p\phi}$ fits the data-set quite well, and returns $D(\phi = 1) \approx 1.6 \cdot 10^{-9} [m^2/s]$. Hence, $D(\phi = 1)$ for PVA-water solution and $D_{s.d.}$ are of the same order of magnitude. Concerning the possible variation of the diffusivity in the hydrating (non-equilibrium) film, in the lack of any local measurement (which would however be not easily done), it is assumed to be neglibigle ($M = 0$ in eq. 3.24).

The value of water diffusion coefficient in the dry side of the film, D_{02}, is chosen small enough to guarantee the stability of the solution, but not too small, to avoid numerical issues in the algorithm. Values of $D_{02}/D_{01} = 10^{-5}$ proved to be the best in terms of robustness of the routine.

Number of sub-chains per unit volume

The number of sub-chains per unit volume N is the only value left as a fitting parameter in the model. It is shown that, on the time scale we are interested in, swelling is not highly affected by N: Fig. 5.14 shows, indeed, that even if this parameter is changed by two orders of magnitude, the impact on the predicted volume increase is negligible, especially when compared to the change in χ. N has been modified in the range $[10^{24} - 10^{26}][m^{-3}]$, an interval considered to be typical for polymer films above the glass transition [56]. The best fit is obtained with a value of $N = 10^{24}[m^{-3}]$ both for film A and B. Dynamic mechanical analysis tests are planned to measure the shear modulus $G = Nk_BT$ for these two films and confirm the choice made for N.

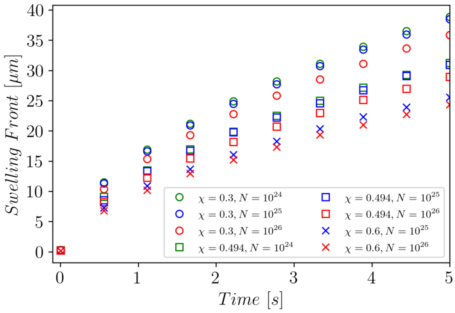

Figure 5.14. Sensitivity Analysis on the model. N and χ are changed in the ranges $[10^{24} - 10^{26}][m^{-3}]$ and $[0.3 - 0.6]$ respectively. The impact on the predicted swelling front at specific times is shown.

5.2.2 Results

The main output of the model implementation is, of course, the water concentration profile as a function of time and position inside the polymer matrix.

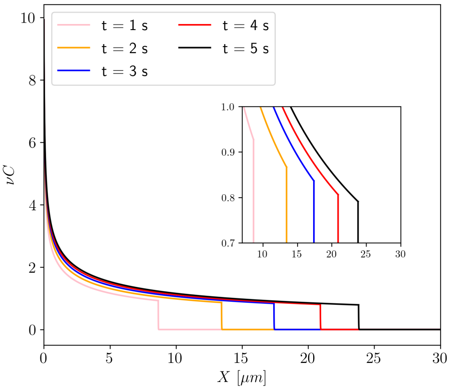

Figure 5.15. Predicted concentration profile for Film A, plotted for $t = 1, 2, 3, 4$ and $5[s]$

In Fig. 5.15 the concentration C multiplied by the volume of a water molecule ν is plotted as a function of the non-eulerian coordinate X for film A. It is here reminded that, in this frame of reference, $X = 0$ will correspond, for any time, to the swelling front; the position of the discontinuity, instead will be a function of time indicated by the symbol $X = X_h$. The inset, that focuses on the area where discontinuity occurs, shows that the concentration on the hydration front, C_h, decreases with time: this is different from Case I diffusion where, as shown in Chapter 3, C_h is constant in time.

The main graph also shows that, especially at long times, the concentration has a huge drop in a small space, after which it decreases with a much lower slope. This resonates with the observations performed by OCT, where the area immediately before the hydration front seems homogeneously black, indicating no change in refractive index (and thus an almost constant concentration).

As mentioned, however, at this stage the model could not be validated on the entire concentration profile, since an experimental setup to measure water content in the film in such a short time was not available to us. The validation, instead, has been done on the position of the swelling front, using Eq. 3.22.

Fig. 5.16 shows the excellent agreement between model prediction and the average swelling as measured by Optical Microscopy.

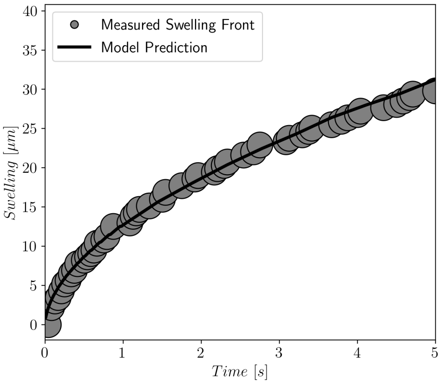

Figure 5.16. Swelling Front as measured by Optical Microscopy (points) and predicted by the model (solid line).

For Film A, the model can also be validated by an independent measure: the water mass absorbed by the film, obtained from STS. Fig. 5.17 shows that, also in this case, the model output reproduces data quite well.

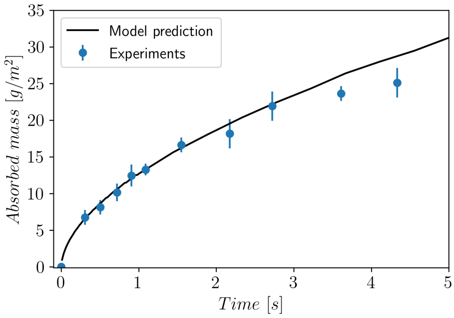

Figure 5.17. Absorbed mass as measured by STS (points) and predicted by the model (solid line).

Analogous results in swelling behaviour is shown in Fig. 5.18 for film B. Absorption curve is not available for this material, but the agreement with swelling performance is again very good.

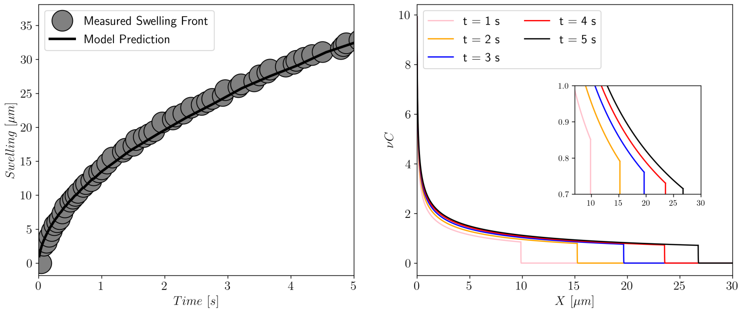

Figure 5.18. Predictions for swelling (left) and concentration profile (right) for film B. Swelling prediction (solid line) is compared with optical microscopy data (points).

CHAPTER 6

Discussion, Conclusions and some Perspectives

The aim of this thesis was to give physical insights on solvent-assisted welding of polymeric films, laying the foundations for a predictive tool for the seal strength. Most of the work has been done on characterizing the diffusion behaviour of water in a Polyvinyl alcohol-based film, and the subsequent deformation of the polymer matrix: the main target application is, indeed, the solvent sealing of polymer films for the production of Laundry Detergent Pods.

By means of optical microscopy, a top view of the process is obtained. Two sharp fronts are clearly visible: the first one represents water diffusion, and has been termed penetration or hydration front; the other one, named swelling front, follows the volume increase of the film. As it is common in this kind of problems, the position of the two fronts have been tracked (by means of image analysis) and monitored as a function of time. Fitting both fronts' positions with a power-law function, the best exponent obtained was included in the interval $[0.51 - 0.65]$, for both analyzed films. Moreover, for each single film the behaviour of the penetration front was significantly different from the one of swelling front. These two features are peculiar of a diffusion/swelling process that is usually termed anomalous.

The top view of the optical microscopy setup allowed for observing diffusion and swelling only along the width of the polymer film. In most applications, including Laundry Detergent Pods' production, however, liquid solvent is applied on top of the film surface, and the process of diffusion and swelling occurs along the depth of the film.

To overcome this limitation of the Optical Microscopy technique, Optical Coherence Tomography has also been used. This interferometric technique, indeed, allows for a reconstruction of the film along its depth even during diffusion, showing the positions of both fronts in the desired direction.

While the two techniques give identical results for the position of the penetration front, differences at longer times are found for the swelling front. Optical microscopy, indeed, shows a plateau starting around 5 seconds; a plateau that is absent in the measurement with Tomography, where the swelling front keeps increasing for the entire duration of the recorded process. These differences, that are to be investigated as a future perspective, have here been disregarded, since the range of times relevant to pods' production is shorter than 5 s. Another interesting feature of Tomography that would be worth investigating is the possibility to directly correlate the pixel intensity with the local solvent content: in this way, the complete concentration profile would be measurable.

In the lack of a direct measure for local concentration, the total absorbed mass of solvent has been measured as a function of time, specifically, for film A, which is the one directly wet in the industrial process. In this way, two independent measurements (swelling front and absorbed mass) were available for model validation for this important case.

In an effort to rationalize and predict experimental results, a new model has also been developed that provides the full concentration profile in the mixtures of liquid solvent-polymers. The model assumes a priori the existence of a sharp penetration front; moreover the position of this front in a lab-fixed frame of reference $x_h(t)$ must be known. Beyond $x_h(t)$, few other parameters are needed, all of them being, in principle, measurable. Two thermodynamic parameters, i.e., the number of polymer sub-chains per unit volume N and the polymer-solvent interaction parameter χ, are needed in the hydrated side, together with the diffusion coefficients in the hydrated and dry regions, $D_1(C)$ and D_{02} respectively.

To predict the behaviour in the system water-PVA, a constant diffusion coefficient equal to the self-diffusivity of water was assumed in the hydrated side, $D_1 = D_{01} = D_{s.d.}$, which was proven to be a good approximation for our system. Moreover, decreasing the ratio $r = D_{02}/D_{01}$ led to convergence of the algorithm in the results for $r = 10^{-5}$: thus, in actual facts, there was no need to measure the diffusion coefficient in the dry side, provided that a large difference between transport properties in hydrated and dry regions of the film can be assumed a priori. Regarding the thermodynamic parameters, $\chi = 0.494$ was used as a reasonable value for our water-PVA system, while N was left as a fitting parameter. As a perspective, the actual value of N could be estimated from the relation $G = Nk_BT$, where the elastic modulus G can be measured, for example, through Dynamic Mechanical Analysis; however, we checked that a change of this parameter by two orders of magnitude has a negligible impact on the predicted swelling, at least on the time-scale we are interested in.

Notice that the value employed for $\chi = 0.494$ is a constant one, as typically found for solutions of water in PVA. Some authors [96, 97] however argued that the actual value of χ should decrease with increasing water content. Since in the original Flory-Huggins theory χ is a constant, and since the agreement between model prediction and experiments is already excellent, the actual dependence $\chi = \chi(C)$ has been here neglected. Even more so, N has been kept constant since, as already discussed, it also has a very low impact on the final predictions.

The developed model has also been applied to data published in literature for systems in which Case I [8] and Case II [12] diffusion type were found. Here, a brief comparison is made between the model introduced in Chapter 3 and the ones presented in the two just mentioned references, i.e., the model by Mao et al. and the one by Thomas and Windle.

The application of our model to Case I followed a similar approach to the the one just described for anomalous diffusion, and the agreement was equally good. Compared to the model by Mao et al., that is a model for Case I diffusion only, the one developed in this work is much more versatile, since, as mentioned, the position of the hydration front could follow any function of time. Despite being more versatile, our theory also needs less parameters than the one by Mao et al.: thermodynamic constants N_d and χ_d in the dry polymer are indeed not needed, since a standard Fickian diffusion equation holds.

To successfully predict Case II behaviour, a constant diffusion coefficient in the hydrated side was not sufficient, and we assumed an exponential dependence of D_1 from water concentration. Even with this choice, the number of parameters needed by our model is still smaller than that needed in the theory by Thomas and Windle. In their equations, indeed, also the film viscosity and its dependence from water concentration are required. However, differently from the model by Mao et al. and from ours, the front position as a function of time will be obtained by Thomas and Windle as an output.

It is here remarked that both those models use the assumption $X_h(t) = x_h(t)$: Thomas and Windle explicitly state that "it is not worth while to correct for increasing thickness of the specimen as swelling proceeds", while Mao et al. use the simplified version of eq. 3.22 to predict the swelling front in the lab-fixed frame, even if no comment is done on this working hypothesis. We have instead commented on this hypothesis in Chapter 3.

Finally, to shed some light on the second step of solvent-assisted sealing of polymer films, T-peel tests measurements have also been performed to measure adhesion strength on-the-fly, which required the development of an adequate protocol to obtain stable and reproducible results. Interestingly, in the wet adhesion process, the effect of the curing time on the peeling force, is not as direct as it would be for a dry sealing, as we demonstrated clearly through some preliminary results. It should be however stressed that the behaviour of the final junction will depend on other operating parameters, like the applied Coat Weight and/or the open time. In this respect, we found an interesting dependence on the open time (i.e., the time given to water for diffusion in the first film before contact) for the peel force, with an unexpected maximum found around an open time of 1.3 s. This confirms that water content at the polymer surface plays a key role for adhesion and that tuning the solvent concentration at the moment of contact between the two films can lead to high quality sealing only by changing the operating conditions.

As a perspective, a wider experimental campaign should be carried out for measuring the peel force and building a predictive tool for the entire process, assessing the role of surface water concentration.

While the solvent absorption process has been modelled by means of continuum mechanics, a microscopic approach would probably be the best way to model the adhesion itself since, as already discussed, the motion of polymer chains plays a key role in this regard. Thus, as a final perspective, the inter-diffusion of polymer chains could also be studied by means of Molecular Dynamics simulations, which will give us the opportunity to exploit the numerical expertise we developed working on different glassy materials [98, 99].

Bibliography

[1] Qian Shi, Kai Yu, Martin L Dunn, Tiejun Wang, and H Jerry Qi. Solvent assisted pressure-free surface welding and reprocessing of malleable epoxy polymers. *Macromolecules*, 49(15):5527–5537, 2016.

[2] Richard AL Jones and Randal W Richards. *Polymers at surfaces and interfaces*. 1999.

[3] Richard P Wool, B-L Yuan, and OJ McGarel. Welding of polymer interfaces. *Polymer Engineering & Science*, 29(19):1340–1367, 1989.

[4] F Beaume and N Brown. Effect of predrying time on the strength of solvent-welded polyamide-11 joints. *The Journal of Adhesion*, 43(1-2):91–100, 1993.

[5] Vijay K Stokes. Joining methods for plastics and plastic composites: an overview. *Polymer Engineering & Science*, 29(19):1310–1324, 1989.

[6] Chunyan Cui and Wenguang Liu. Recent advances in wet adhesives: Adhesion mechanism, design principle and applications. *Progress in Polymer Science*, 116:101388, 2021.

[7] Hyunwoo Yuk, Claudia E Varela, Christoph S Nabzdyk, Xinyu Mao, Robert F Padera, Ellen T Roche, and Xuanhe Zhao. Dry double-sided tape for adhesion of wet tissues and devices. *Nature*, 575(7781):169–174, 2019.

[8] Xinyu Mao, Hyunwoo Yuk, and Xuanhe Zhao. Hydration and swelling of dry polymers for wet adhesion. *Journal of the Mechanics and Physics of Solids*, 137:103863, 2020.

[9] John Crank. *The mathematics of diffusion*. Oxford university press, 1979.

[10] S Bargmann, AT McBride, and P Steinmann. Models of solvent penetration in glassy polymers with an emphasis on case ii diffusion. a comparative review. *Applied Mechanics Reviews*, 64(1), 2011.

[11] Masao Doi, Samuel Frederick Edwards, and Samuel Frederick Edwards. *The theory of polymer dynamics*, volume 73. oxford university press, 1988.

[12] Noreen L Thomas and AH Windle. A theory of case ii diffusion. *Polymer*, 23(4):529–542, 1982.

[13] D De Kee, Q Liu, and J Hinestroza. Viscoelastic (non-fickian) diffusion. *The Canadian Journal of Chemical Engineering*, 83(6):913–929, 2005.

[14] D Vesely. Diffusion of liquids in polymers. *International Materials Reviews*, 53(5):299–315, 2008.

[15] CE Rogers. Physics and chemistry of the organic solid state. *John Wiley & Sons, Inc., New York*, 2, 1965.

[16] G S Park. Transport principles—solution, diffusion and permeation in polymer membranes. *Synthetic membranes: Science, engineering and applications*, pages 57–107, 1986.

[17] GK Van der Wel and OCG Adan. Moisture in organic coatings—a review. *Progress in organic coatings*, 37(1-2):1–14, 1999.

[18] Partho Neogi. *Diffusion in polymers*, volume 32. CRC Press, 1996.

[19] HL Frisch. Sorption and transport in glassy polymers–a review. *Polymer Engineering & Science*, 20(1):2–13, 1980.

[20] M A Del Nobile, G Mensitieri, P A Netti, and L Nicolais. Anomalous diffusion in poly-ether-ether-ketone. *Chemical engineering science*, 49(5):633–644, 1994.

[21] Ruben G Carbonell and Giulio C Sarti. Coupled deformation and mass-transport processes in solid polymers. *Industrial & engineering chemistry research*, 29(7):1194–1204, 1990.

[22] PH Hermans. Contributions to the physics of cellulose fibers elsevier. *Amsterdam, The Netherlands*, 1946.

[23] GS Hartley. Diffusion and swelling of high polymers. part i.—the swelling and solution of a high polymer solid considered as a diffusion process. *Transactions of the Faraday Society*, 42:B006–B011, 1946.

[24] Conmar Robinson. Diffusion and swelling of high polymers. part ii. the orientation of polymer molecules which accompanies unidirectional diffusion. *Transactions of the Faraday Society*, 42:B012–B017, 1946.

[25] GS Hartley. Diffusion and swelling of high polymers. part iii.—anisotropic swelling in oriented polymer film. *Transactions of the Faraday Society*, 45:820–832, 1949.

[26] M Sanopoulou and JH Petropoulos. Phenomenology and mechanisms of unidimensional stress-dependent micromolecular transport in a stiff-chain polymer. ii. uniaxially oriented cellulose acetate. *Journal of Polymer Science Part B: Polymer Physics*, 30(9):983–992, 1992.

[27] Christopher J Durning and William B Russel. A mathematical model for diffusion with induced crystallization: 2. *Polymer*, 26(1):131–140, 1985.

[28] JH Petropoulos and M Sanopoulou. Test of a model of stress-dependent diffusion by means of combined colored tracer and birefringence profile measurements. *Journal of Polymer Science Part B: Polymer Physics*, 26(5):1087–1099, 1988.

[29] JS Vrentas, CM Vrentas, and WJ Huang. Anticipation of anomalous effects in differential sorption experiments. *Journal of applied polymer science*, 64(10):2007–2013, 1997.

[30] Turner Alfrey Jr, EF Gurnee, and WG Lloyd. Diffusion in glassy polymers. In *Journal of Polymer Science Part C: Polymer Symposia*, volume 12, pages 249–261. Wiley Online Library, 1966.

[31] Noreen Thomas and AH Windle. Transport of methanol in poly (methyl methacrylate). *Polymer*, 19(3):255–265, 1978.

[32] D Vesely. The rate of solvent diffusion in amorphous polymers. In *Macromolecular Symposia*, volume 138, pages 215–223. Wiley Online Library, 1999.

[33] G Camera-Roda and GC Sarti. Non-fickian mass transport through polymers: a viscoelastic theory. *Transport theory and statistical physics*, 15(6-7):1023–1050, 1986.

[34] Mohammad Karimi. Diffusion in polymer solids and solutions. *Mass transfer in chemical engineering processes*, 25:17, 2011.

[35] JS Vrentas, CM Jarzebski, and JL Duda. A deborah number for diffusion in polymer-solvent systems. *AIChE Journal*, 21(5):894–901, 1975.

[36] JS Vrentas and JL Duda. Diffusion in polymer–solvent systems. iii. construction of deborah number diagrams. *Journal of Polymer Science: Polymer Physics Edition*, 15(3):441–453, 1977.

[37] Nikolaos S Kalospiros, Raffaella Ocone, Gianni Astarita, and Jerry H Meldon. Analysis of anomalous diffusion and relaxation in solid polymers. *Industrial & engineering chemistry research*, 30(5):851–864, 1991.

[38] Giovanni Camera-Roda and Giulio C Sarti. Mass transport with relaxation in polymers. *AIChE journal*, 36(6):851–860, 1990.

[39] Balaji Narasimhan and Nikolaos A Peppas. On the importance of chain reptation in models of dissolution of glassy polymers. *Macromolecules*, 29(9):3283–3291, 1996.

[40] Ping I Lee and Nikolaos A Peppas. Prediction of polymer dissolution in swellable controlled-release systems. *Journal of Controlled Release*, 6(1):207–215, 1987.

[41] Beth A Miller-Chou and Jack L Koenig. A review of polymer dissolution. *Progress in polymer science*, 28(8):1223–1270, 2003.

[42] Adolph Fick. On liquid diffusion. *The London, Edinburgh, and Dublin Philosophical Magazine and Journal of Science*, 10(63):30–39, 1855.

[43] J Crank. A theoretical investigation of the influence of molecular relaxation and internal stress on diffusion in polymers. *Journal of Polymer Science*, 11(2):151–168, 1953.

[44] JH Petropoulos. Interpretation of anomalous sorption kinetics in polymer-penetrant systems in terms of a time-dependent solubility coefficient. *Journal of Polymer Science: Polymer Physics Edition*, 22(11):1885–1900, 1984.

[45] M Sanopoulou, DF Stamatialis, and JH Petropoulos. Investigation of case ii diffusion behavior. 1. theoretical studies based on the relaxation dependent solubility model. *Macromolecules*, 35(3):1012–1020, 2002.

[46] AH Windle. Case ii sorption. In *Polymer Permeability*, pages 75–118. Springer, 1985.

[47] CJ Durning. Differential sorption in viscoelastic fluids. *Journal of Polymer Science: Polymer Physics Edition*, 23(9):1831–1855, 1985.

[48] CJ Durning and M Tabor. Mutual diffusion in concentrated polymer solutions under a small driving force. *Macromolecules*, 19(8):2220–2232, 1986.

[49] C-Y Hui, K-C Wu, Ronald C Lasky, and Edward J Kramer. Case-ii diffusion in polymers. i. transient swelling. *Journal of Applied Physics*, 61(11):5129–5136, 1987.

[50] C-Y Hui, K-C Wu, Ronald C Lasky, and Edward J Kramer. Case-ii diffusion in polymers. ii. steady-state front motion. *Journal of Applied Physics*, 61(11):5137–5149, 1987.

[51] Tiezheng Qian and PL Taylor. From the thomas–windle model to a phenomenological description of case-ii diffusion in polymers. *Polymer*, 41(19):7159–7163, 2000.

[52] G Astarita and GC Sarti. A class of mathematical models for sorption of swelling solvents in glassy polymers. *Polymer Engineering & Science*, 18(5):388–395, 1978.

[53] Shawn A Chester and Lallit Anand. A coupled theory of fluid permeation and large deformations for elastomeric materials. *Journal of the Mechanics and Physics of Solids*, 58(11):1879–1906, 2010.

[54] Shawn A Chester. A constitutive model for coupled fluid permeation and large viscoelastic deformation in polymeric gels. *Soft Matter*, 8(31):8223–8233, 2012.

[55] Nikolaos Bouklas and Rui Huang. Swelling kinetics of polymer gels: comparison of linear and nonlinear theories. *Soft Matter*, 8(31):8194–8203, 2012.

[56] Wei Hong, Xuanhe Zhao, Jinxiong Zhou, and Zhigang Suo. A theory of coupled diffusion and large deformation in polymeric gels. *Journal of the Mechanics and Physics of Solids*, 56(5):1779–1793, 2008.

[57] Fernando P Duda, Angela C Souza, and Eliot Fried. A theory for species migration in a finitely strained solid with application to polymer network swelling. *Journal of the Mechanics and Physics of Solids*, 58(4):515–529, 2010.

[58] Masao Doi. Gel dynamics. *Journal of the Physical Society of Japan*, 78(5):052001, 2009.

[59] Paul J Flory. *Principles of polymer chemistry*. Cornell university press, 1953.

[60] Sanjay Govindjee and Juan C Simo. Coupled stress-diffusion: Case ii. *Journal of the Mechanics and Physics of Solids*, 41(5):863–887, 1993.

[61] Prashanth K Vijalapura and Sanjay Govindjee. Numerical simulation of coupled-stress case ii diffusion in one dimension. *Journal of Polymer Science Part B: Polymer Physics*, 41(18):2091–2108, 2003.

[62] Liliane Léger and Costantino Creton. Adhesion mechanisms at soft polymer interfaces. *Philosophical Transactions of the Royal Society A: Mathematical, Physical and Engineering Sciences*, 366(1869):1425–1442, 2008.

[63] Lu Gong, Li Xiang, Jiawen Zhang, Jingsi Chen, and Hongbo Zeng. Fundamentals and advances in the adhesion of polymer surfaces and thin films. *Langmuir*, 35(48):15914–15936, 2019.

[64] Guido Raos and Bruno Zappone. Polymer adhesion: Seeking new solutions for an old problem#. *Macromolecules*, 54(23):10617–10644, 2021.

[65] Firas Awaja, Michael Gilbert, Georgina Kelly, Bronwyn Fox, and Paul J Pigram. Adhesion of polymers. *Progress in polymer science*, 34(9):948–968, 2009.

[66] Zeqian Sun, Zhenghao Li, Keyu Qu, Zongzheng Zhang, Yuzhong Niu, Wenlong Xu, and Chunguang Ren. A review on recent advances in gel adhesion and their potential applications. *Journal of Molecular Liquids*, 325:115254, 2021.

[67] Mohammed Panthakkal Abdul Muthalif and Youngson Choe. Adhesive and impact-peel strength improvement of epoxy resins modified with mono and diamine functionalized elastomers. *Advances in Polymer Technology*, 2022, 2022.

[68] Young Hwa Kim and Richard P Wool. A theory of healing at a polymer-polymer interface. *Macromolecules*, 16(7):1115–1120, 1983.

[69] K Jud, HH Kausch, and JG Williams. Fracture mechanics studies of crack healing and welding of polymers. *Journal of Materials Science*, 16:204–210, 1981.

[70] Ingo Müller and Tommaso Ruggeri. *Rational extended thermodynamics*, volume 37. Springer Science & Business Media, 2013.

[71] R Byron Bird. Transport phenomena. *Appl. Mech. Rev.*, 55(1):R1–R4, 2002.

[72] Lev Davidovich Landau and Evgenii Mikhailovich Lifshitz. *Fluid Mechanics: Landau and Lifshitz: Course of Theoretical Physics, Volume 6*, volume 6. Elsevier, 2013.

[73] C Truesdell and W Noll. *The non-linear field theories of mechanics*. Springer, 2004.

[74] Eduardo A de Souza Neto, Djordje Peric, and David RJ Owen. *Computational methods for plasticity: theory and applications*. John Wiley & Sons, 2011.

[75] J Rehner. Statistical mechanics of cross-linked polymer networks. ii. swelling. *J Chem Phys*, 11:521–6, 1943.

[76] Terrell L Hill. *An introduction to statistical thermodynamics*. Courier Corporation, 1986.

[77] Masao Doi. *Introduction to polymer physics*. Oxford university press, 1996.

[78] Pauli Virtanen, Ralf Gommers, Travis E. Oliphant, Matt Haberland, Tyler Reddy, David Cournapeau, Evgeni Burovski, Pearu Peterson, Warren Weckesser, Jonathan Bright, Stéfan J. van der Walt, Matthew Brett, Joshua Wilson, K. Jarrod Millman, Nikolay Mayorov, Andrew R. J. Nelson, Eric Jones, Robert Kern, Eric Larson, C J Carey, İlhan Polat, Yu Feng, Eric W. Moore, Jake VanderPlas, Denis Laxalde, Josef Perktold, Robert Cimrman, Ian Henriksen, E. A. Quintero, Charles R. Harris, Anne M. Archibald, Antônio H. Ribeiro, Fabian Pedregosa, Paul van Mulbregt, and SciPy 1.0 Contributors. SciPy 1.0: Fundamental Algorithms for Scientific Computing in Python. *Nature Methods*, 17:261–272, 2020.

[79] Jakob Nixdorf, Giuseppe Di Florio, Lars Broöckers, Carolin Borbeck, Helen E Hermes, Stefan U Egelhaaf, and Peter Gilch. Uptake of methanol by poly (methyl methacrylate): an old problem addressed by a novel raman technique. *Macromolecules*, 52(13):4997–5005, 2019.

[80] P Colombo, R Bettini, P Santi, A De Ascentiis, and NA Peppas. Analysis of the swelling and release mechanisms from drug delivery systems with emphasis on drug solubility and water transport. *Journal of controlled release*, 39(2-3):231–237, 1996.

[81] Narendra Krishna and Frank Brow. Polyvinyl alcohol as an ophthalmic vehicle: Effect on regeneration of corneal epithelium. *American Journal of Ophthalmology*, 57(1):99–106, 1964.

[82] Reza Abedi-Firoozjah, Negar Chabook, Omid Rostami, Mahshid Heydari, Azin Kolahdouz-Nasiri, Fardin Javanmardi, Khadije Abdolmaleki, and Amin Mousavi Khaneghah. Pva/starch films: An updated review of their preparation, characterization, and diverse applications in the food industry. *Polymer Testing*, page 107903, 2022.

[83] Herman S Mansur, Rodrigo L Oréfice, and Alexandra AP Mansur. Characterization of poly (vinyl alcohol)/poly (ethylene glycol) hydrogels and pva-derived hybrids by small-angle x-ray scattering and ftir spectroscopy. *Polymer*, 45(21):7193–7202, 2004.

[84] Maribel I Baker, Steven P Walsh, Zvi Schwartz, and Barbara D Boyan. A review of polyvinyl alcohol and its uses in cartilage and orthopedic applications. *Journal of Biomedical Materials Research Part B: Applied Biomaterials*, 100(5):1451–1457, 2012.

[85] Di Zhang, Wei Zhou, Bing Wei, Xin Wang, Rupei Tang, Jiemin Nie, and Jun Wang. Carboxyl-modified poly (vinyl alcohol)-crosslinked chitosan hydrogel films for potential wound dressing. *Carbohydrate polymers*, 125:189–199, 2015.

[86] AB Norton, RD Hancocks, and LM Grover. Poly (vinyl alcohol) modification of low acyl gellan hydrogels for applications in tissue regeneration. *Food Hydrocolloids*, 42:373–377, 2014.

[87] G. Bradski. The OpenCV Library. *Dr. Dobb's Journal of Software Tools*, 2000.

[88] Jianing Yao and Jannick P Rolland. Optical coherence tomography for polymer film evaluation. In *Optical Coherence Tomography and Its Non-medical Applications*. IntechOpen, 2020.

[89] Elke C Sattler, Raphaela Kästle, and Julia Welzel. Optical coherence tomography in dermatology. *Journal of biomedical optics*, 18(6):061224, 2013.

[90] Teresa C Chen, Ambika Hoguet, Anna K Junk, Kouros Nouri-Mahdavi, Sunita Radhakrishnan, Hana L Takusagawa, and Philip P Chen. Spectral-domain oct: helping the clinician diagnose glaucoma: a report by the american academy of ophthalmology. *Ophthalmology*, 125(11):1817–1827, 2018.

[91] Michael R Wang. *Optical Coherence Tomography and Its Non-medical Applications*. 2020.

[92] Silke Aumann, Sabine Donner, Jörg Fischer, and Frank Müller. Optical coherence tomography (oct): principle and technical realization. *High Resolution Imaging in Microscopy and Ophthalmology*, pages 59–85, 2019.

[93] James E Mark et al. *Physical properties of polymers handbook*, volume 1076. Springer, 2007.

[94] Ichiro Sakurada, Akio Nakajima, and Hiroyuki Fujiwara. Vapor pressures of polymer solutions. ii. vapor pressure of the poly(vinyl alcohol)-water system. *Journal of Polymer Science*, 35(129):497–505, 1959.

[95] M Holz S Heil A Sacco. Temperature-dependent self-diausion coefficients of water and six selected molecular liquids for calibration in accurate 1h nmr pfg measurements. *Phys. Chem. Chem. Phys*, 2:4740–4742, 2000.

[96] Gregory B McKenna and Ferenc Horkay. Effect of crosslinks on the thermodynamics of poly (vinyl alcohol) hydrogels. *Polymer*, 35(26):5737–5742, 1994.

[97] Nikolaos A Peppas and Edward W Merrill. Determination of interaction parameter $\chi 1$, for poly (vinyl alcohol) and water in gels crosslinked from solutions. *Journal of Polymer Science: Polymer Chemistry Edition*, 14(2):459–464, 1976.

[98] G Porpora, F Rusciano, V Guida, F Greco, and R Pastore. Understanding charged vesicle suspensions as wigner glasses: dynamical aspects. *Journal of Physics: Condensed Matter*, 33(10):104001, 2020.

[99] Giuseppe Porpora, Francesco Rusciano, Raffaele Pastore, and Francesco Greco. Comparing microscopic and macroscopic dynamics in a paradigmatic model of glass-forming molecular liquid. *International Journal of Molecular Sciences*, 23(7):3556, 2022.

Author's Publications

- Giuseppe Porpora, Francesco Rusciano, Vincenzo Guida, Francesco Greco, and Raffaele Pastore. Understanding charged vesicle suspensions as wigner glasses: dynamical aspects. Journal of Physics: Condensed Matter, 33(10):104001, 2020.
- Giuseppe Porpora, Francesco Rusciano, Raffaele Pastore, and Francesco Greco. Comparing microscopic and macroscopic dynamics in a paradigmatic model of glass-forming molecular liquid. International Journal of Molecular Sciences, 23(7):3556, 2022.